HIGH MAGNETIC FIELD MEASUREMENTS ON SINTERED $SmCo_5$ PERMANENT MAGNETS

STANLEY R. TROUT

A THESIS

IN

METALLURGY AND MATERIALS SCIENCE

Presented to the Faculty of the College of Engineering and Applied Science of The University of Pennsylvania in partial fulfillment of the requirements for the degree

MASTER OF SCIENCE

1976

C. D. Graham, Jr.
Supervisor

C. Laird
Graduate Group Chairman

ABSTRACT

Hysteresis loops in fields to 100 kOe have been measured at 300, 77, and 4.2 K parallel and perpendicular to the alignment axis in a series of sintered $SmCo_5$ permanent magnets. The samples include a series with compositions varying from 16.24 to 17.08 atomic percent samarium, prepared and measured at room temperature by Martin, Benz, and Rockwood,[1] as well as two samples from Hitachi Metals, Ltd., Japan.

A statistical model is developed to describe the orientation of particle easy axes with respect to the alignment direction in sintered $SmCo_5$ magnets. The two-dimensional orientation distribution measured metallographically by Martin[2] is predicted by projecting the proposed distribution onto a plane. For a given particle distribtuion, the model predicts the ratio of remanence to saturation, and also the shape of the magnetization curve measured in decreasing fields when the field is applied either parallel or perpendicular to the alignment axis. The numerical value of the anisotropy constant and the standard deviation of particle orientations can be determined by comparison of experimental and calculated curves.

Measured intrinsic coercive fields varied from 0.34 to 42.2 kOe while the anisotropy varied from 6×10^7 to 1.6×10^8 ergs/cm^3 at room temperature. In all samples, H_{ci} and con-

sequently (BH)max increased linearly as the temperature decreased, confirming more generally the result reported for a single sample by Benz and Martin.[3] The anisotropy increased as the temperature decreased to 77 K, but then either decreased or increased, depending on the composition of the sample, when the temperature was lowered to 4.2 K. At all temperatures, permanent magnet properties peak near 16.8 atomic percent samarium, and seem to correlate with the degree of particle alignment for the samples from Martin et al.[1] The results generally confirm the view that the coercive field in sintered $SmCo_5$ magnets is controlled by changes in microstructure and not by changes in bulk properties such as anisotropy.

TABLE OF CONTENTS

LIST OF FIGURES, TABLES, AND PROGRAMS

I. INTRODUCTION

The history of rare earth-cobalt permanent magnets can be traced back to 1935 when Urbain, Weiss, and Trombe[4] discovered that gadolinium is ferromagnetic. At that time, it was difficult to study the magnetic properties of other Lanthanide series elements due to the unavailability of pure rare earth metals. During the Atomic Energy Program, 1942 to 1952, the methods were developed for refining the rare earth elements from their ores. Nassau, Cherry, and Wallace[5] in 1960, used x-ray diffraction methods to determine the crystal structure of the RCo_5 compounds, where R is yttrium or a rare earth element. They found all the RCo_5 compounds to have the $CaCu_5$ crystal structure which is shown in figure 1 for $SmCo_5$. The anisotropy energy in hexagonal materials is defined by $E_K=K_1\sin^2\theta+K_2\sin^4\theta$, where θ is the angle between the saturation magnetization M_s and the c axis of the crystal. (Magnetic parameters are defined in figure 2.) Also, in 1960 Hubbard, Adams, and Gilfrich[6] reported the permanent magnet properties of $GdCo_5$. They related the large magnetocrystalline anisotropy to the huge coercivity. The easy magnetic axis was found to be parallel to the hexagonal c axis and particle alignment was used to increase the magnetization. Initially, their work was ignored due to the high cost of gadolinium and it was not recognized that $GdCo_5$ is one of a family of compounds. Hoffer and Strnat[7]

reported the large magnetocrystalline anisotropy of YCo_5 in 1966. Their work prompted examination of the permanent magnet properties of the RCo_5 compounds, YCo_5, $SmCo_5$, $LaCo_5$, $NdCo_5$, $PrCo_5$, and mischmetal-Co_5.[8] A summary of the magnetic properties of some of these compounds is shown in Table 1.

Of all the RCo_5 compounds, $SmCo_5$ is the best material for use as a permanent magnet for two major reasons:

1. $SmCo_5$ has the highest Curie temperature, T_c=997 K;
2. $SmCo_5$ has the highest anisotropy, $K_1 \sim 10^8$ ergs/cm^3 at room temperature, and K_1 is not very dependent on composition.

In commercial processes, it is common to find sintered $SmCo_5$ magnets with nearly the theoretical (BH)max, that is, H_{ci} is much greater than $4\pi M_s$.

One objectionable point about $SmCo_5$ is that its saturation magnetization is lower than other RCo_5 compounds and some conventional permanent magnet materials as shown in figure 3. To overcome this problem, praseodymium can be substituted for samarium in $SmCo_5$ to achieve a magnet with a larger saturation. A disadvantage of rare earth-cobalt magnets at present, is their high cost. This due mainly to the high cost of rare earth elements. As demand for rare earth-cobalt magnets increases, the economies of scale should cause the price of the magnets to decrease relative to Alnico and other competing magnets. For a given application, the large coercivity of $SmCo_5$ generally means that less material is required than if Alnico were used.

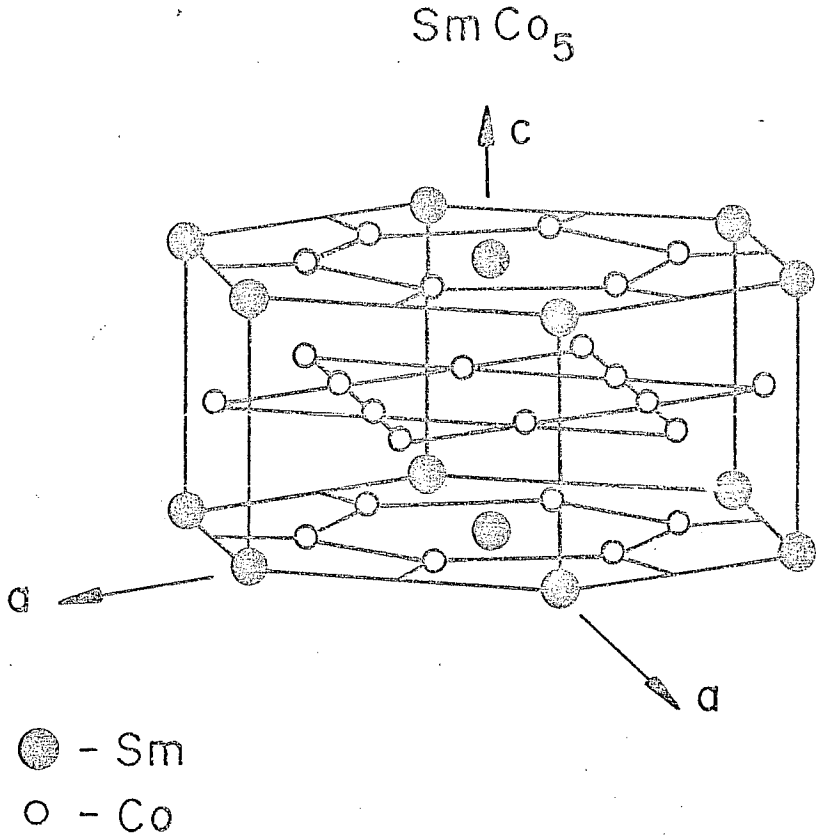

Figure 1. Crystal structure of $SmCo_5$.

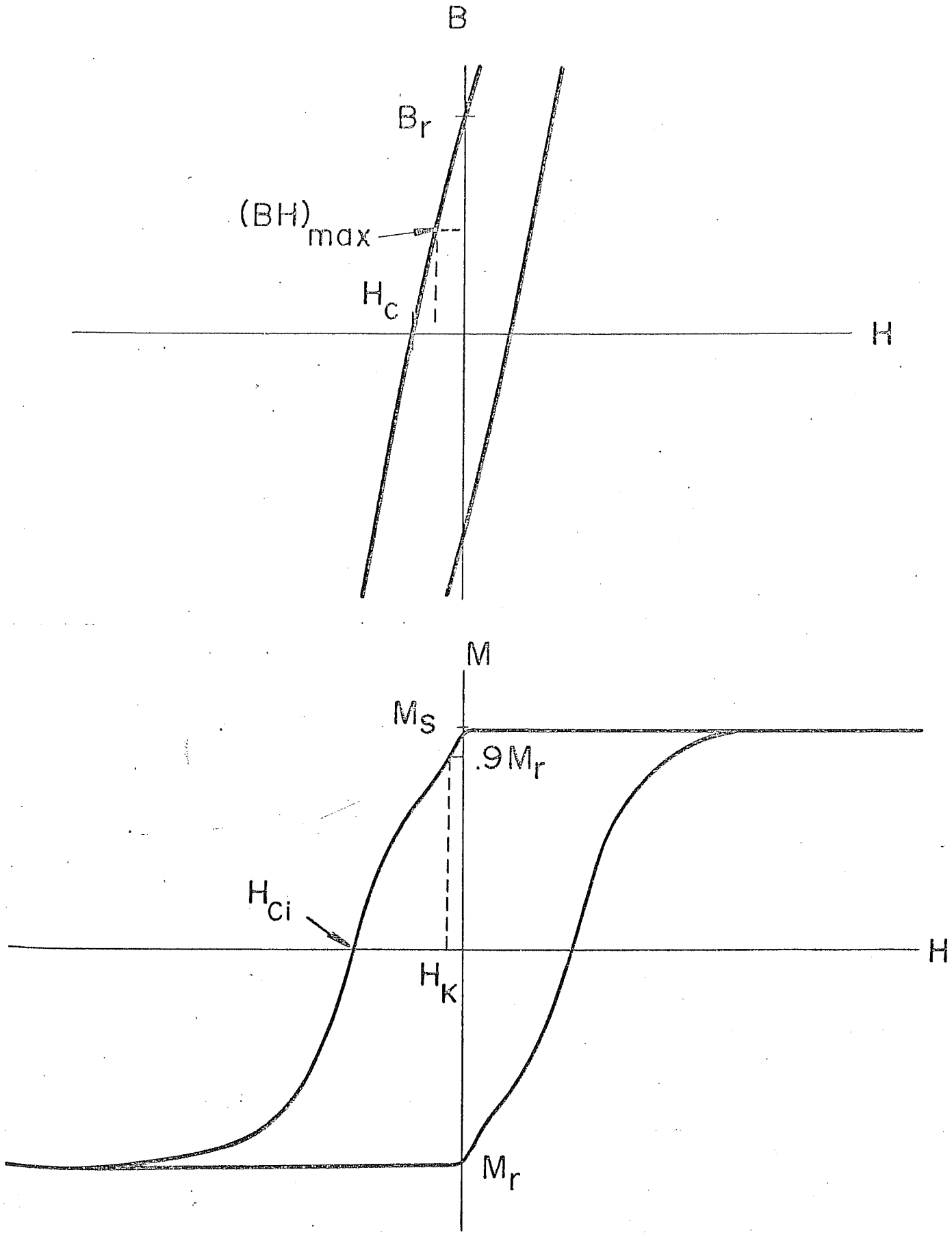

Figure 2. Definition of magnetic parameters.

TABLE 1

MAGNETIC AND PHYSICAL PROPERTIES OF SOME RCo_5 PHASES

Phase	T_C (K)	M_s (emu/cm^3)	(BH)max (MGOe)	H_A (kOe)	K_1 ($x10^7 ergs/cm^3$)	Density (g/cm^3)	T_1 (K)	T_p (K)
YCo_5	921	844	28.1	130	5.5	7.69	1635	1625
$LaCo_5$	840	723	20.6	175	6.3	8.03	1490	1363
$CeCo_5$	647	612	14.8	170-210	5.2-6.4	8.55	1480	1469
$PrCo_5$	885	955	36.0	145-210	6.9-10.0	8.34	1520	1505
$SmCo_5$	997	768	23.0	210-290	8.1-11.2	8.60	1600	1593
$(MM)Co_5$	795	708	19.8	180-195	6.4-6.9	8.35	-	1458

(MM) = mischmetal; properties are for a commercial MM containing, in atomic percent, 54.4% Ce, 26% La, 13% Nd, and 5% Pr.

T_C = Curie temperature

T_1 = liquidus temperature

T_p = temperature of peritectic reaction

(BH)max is calculated from $(4\pi M_s)^2/4$.

(reference 9)

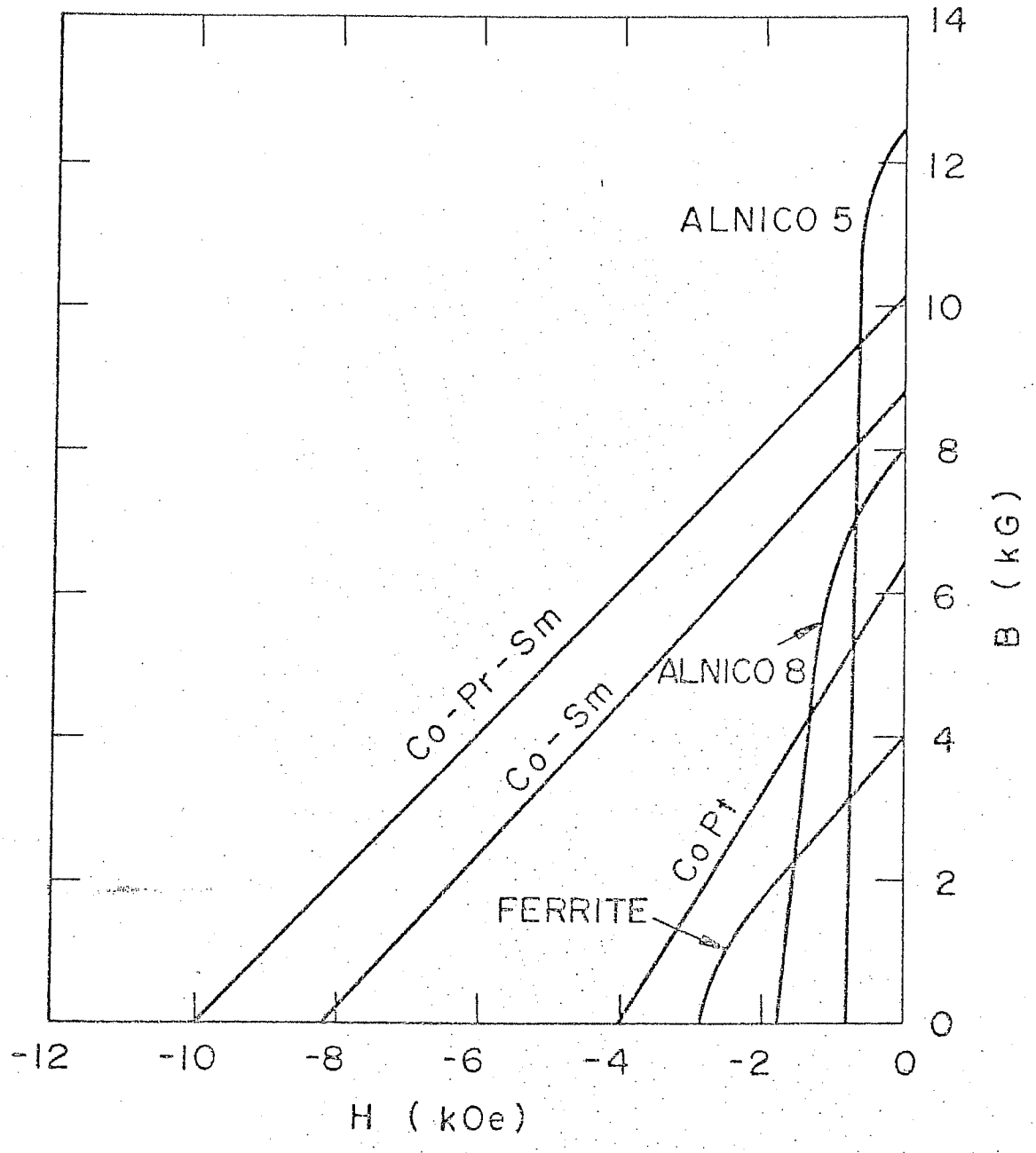

Figure 3. Permanent magnet materials.[8]

At present, the observed intrinsic coercive field of sintered $SmCo_5$ is about an order of magnitude less than the predicted theoretical limit of $2K_1/M_s$ (~ 350 kOe at room temperature). The lower than predicted coercive field of $SmCo_5$ can be explained by the heterogeneous nucleation of reverse domain walls. The three possible sites for domain wall nucleation pointed out in a review by Livingston[10] are:

1. Sharp corners or pits where the local demagnetizing field is high;
2. Regions where K_1 is lowered from either cobalt-rich areas or local elastic strains;
3. Stacking faults.

In sintered magnets, the coercivity depends on composition, sintering temperature and time, and post-sintering heat treatment.

Benz and Martin[3] have examined the temperature dependence of the intrinsic coercive field, H_{ci}, and the anisotropy for a sample of sintered $SmCo_5$ by measuring hysteresis loops parallel and perpendicular to the sample easy axis at 4.2, 77, 300, and 500 K. The sample had a average composition of 16.7 atomic percent samarium. The order of measurement used by Benz and Martin is important to note as it affected their results and conclusions. The sequence of testing was: i) magnetize the sample parallel to its easy axis at 300 K; ii) measure the magnetization of the sample parallel to its easy axis at the temperature of interest, 4.2, 77, 300 or 500 K; iii) remagnetize the sample parallel to its easy axis at 300 K; iv) without demagnetizing, measure the magnetization of the sample perpendicular

to its easy axis at the temperature of interest as a function of increasing field. This method of measurement is reported to lead to linear hard axis magnetization curves, since the samples have no moment perpendicular to the easy axis before any field is applied. Using this type of magentization curve to measure the anisotropy field and hence the anisotropy constant is not accurate, since the particles in the sample are not all perfectly aligned. A different method for finding the anisotropy constant in aligned polycrystalline samples was developed in this research. It is based on a physical model of the magnetization process and is fully described in Section D of Chapter III.

The linear hard axis magnetization curves measured by Benz and Martin are shown in figure 4. Other results of their work are included with the results of this work, figures 13, 15, and 17. They found H_{ci} to increase linearly with decreasing temperature to a value of 52.7 kOe at 77 K, and then decrease slightly to 52.0 kOe at 4.2 K. The anisotropy showed similar behavior increasing linearly to 19.8×10^7 ergs/cm^3 at 77 K and decreasing to 18.9×10^7 ergs/cm^3 at 4.2 K. Their work showed two important points and provided the motivation for this research. First, the anisotropy at 300 K agreed with studies on single crystals, but a different temperature dependence was observed for the sintered alloys. Second, the intrinsic coercivity and the anisotropy were observed to have the same temperature dependence, which is generally not the case.

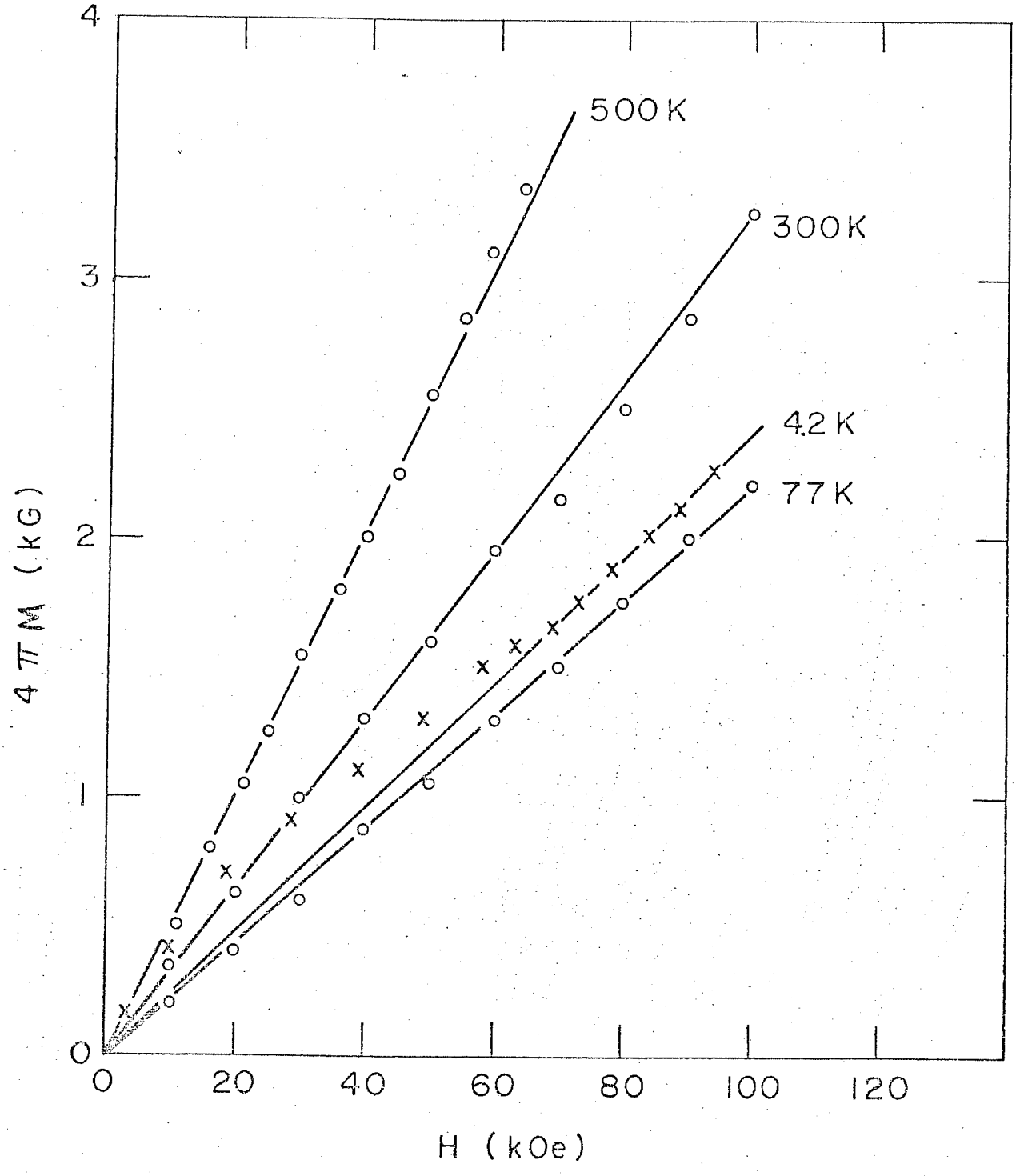

Figure 4. Magnetization of the sample measured perpendicular to the c axis as a function of field applied perpendicular to the c axis, from Benz and Martin.[3]

If H_{ci} is controlled by a domain wall nucleation or pinning event, it is reasonable that H_{ci} would have the same temperature dependence as the domain wall energy, which would be approximately the temperature dependence of $K_1^{\frac{1}{2}}$ neglecting thermal activation effects. To determine if the magnitude of H_{ci} correlates with the magnitude of K_1, measurements on at least two samples are necessary.

The present investigation was undertaken to see whether this temperature dependence of H_{ci} is general for sintered $SmCo_5$ magnets, and more broadly to add to the understanding of the coercive field and other permanent magnet properties of $SmCo_5$ and related materials.

II. SAMPLES

The samples used for this research came from two sources. Dr. D. L. Martin at the General Electric Research and Development Center supplied a set of six samples varying in samarium content from 16.24 to 17.08 atomic percent Sm ($SmCo_{5.16}$ to $SmCo_{4.85}$). These are some of the same samples whose room temperature magnetic properties and lattice parameters were reported by Martin, Benz, and Rockwood;[1] the samples show a wide range of quality as permanent magnets. Two other samples were supplied by Hitachi Metals, Ltd., of Japan. One sample was $SmCo_5$ while the other had some gadolinium added.

The procedure for making sintered $SmCo_5$ magnets is generally the same except for minor variations. The process used by Martin in making the General Electric samples is as follows.[11] Pure samarium and pure cobalt are blended and induction melted to form two different alloys, one nearly $SmCo_5$ and the other samarium-rich $SmCo_5$. The composition, in atomic percent, of the two alloys used by Martin is,

	Co	Sm	O_2	Ni	Al
Alloy A	82.4	16.7	0.68	0.067	0.14
Alloy B	61.4	36.4	2.18	0.028	0.037

The O_2 is assumed to have combined with the available Sm to form Sm_2O_3. Thus the Sm that is assumed to form an oxide

is subtracted from the total Sm to calculate the amount of samarium in $SmCo_x$. The two alloys are ground into powders containing particles with an average diameter of 10 microns. The two powders are blended in the proper proportions to attain a given atomic percent of samarium. Generally, each particle is a single crystal and is free to rotate in the powder. A magnetic field of 60 kOe is applied to the mixture; the easy axis of the particle, the c axis of the $CaCu_5$ crystal structure, (see figure 1) rotates to become approximately parallel to the applied field. The powder is pressed slightly to prevent the particles from rotating out of alignment as the aligning field is removed. Then the powder is pressed to 200,000 psi (1.38×10^9 N/m^2) and then sintered at 1173 K for 30 minutes in an argon atmosphere to form a working magnet with uniaxial symmetry. The composition of alloy B is chosen so that it has a liquid-phase component at the sintering temperature of 1173 K, hence the process is called liquid-phase sintering.[12]

III. MEASUREMENTS

A. General

Magnetization curves and hysteresis loops were measured parallel and perpendicular to the alignment axis in fields up to 105 kOe in the one inch bore Bitter magnet of the Laboratory for Research on the Structure of Matter. A mechanically driven vibrating sample magnetometer was used at a frequency of 4.2 Hz. The samples were cut into cubes approximately 3.2 mm on an edge. The demagnetizing factor was taken to be $4\pi/3$, a value confirmed by measurements on an iron cube of similar dimensions. The correction due to the demagnetizing field is small. A fixed temperature dewar was used for measurements at 300, 77, and 4.2 K; a variable temperature dewar was used for intermediate temperatures.

B. Easy Axis Measurements

The easy axis curves were used to determine the standard permanent magnet properties such as saturation magnetization, remanence, the intrinsic coercive field and the maximum energy product, (BH)max. To simplify the calculation of these quantities, a computer program was developed to correct for the demagnetizing field and to calculate the magnetic properties from data measured directly from the magnetization curve. A listing of the program and a flow chart to explain how the program works are shown in program 1.

PROGRAM 1

```
5 REM MAGNETIC DATA,EASY AXIS, M(J) SWEEP
8 DIM T(100),B(100),H(100),M(100)
10 PRINT "ENTER NAME &TEMP.";\INPUT N1,T
20 READ I,V,I1,K,H(0),N,X
85 Q=INT(90*I1+.5)/10
90 PRINT "ENTER H(";Q;")";\INPUT H(Q)
95 PRINT "ENTER END POINTS OF SWEEP";\INPUT Q1,Q2
100 V1=.03066
101 Z=12.566
105 Y=INT(3428*V1/(V*I)*10+.5)/10
110 FOR J=Q1 TO Q2
115 PRINT "M(";J;")=";\INPUT M(J)
120 B(J)=(Z-N)*M(J)*Y-.1*J*X
125 T(J)=.1*J*X+N*M(J)*Y
127 IF J=Q1GO TO 145
130 IF B(J)*T(J)<B(J-1)*T(J-1)GO TO 165
145 NEXT J
165 T(Q)=H(Q)*X+N*Q*Y*.1
170 M=INT(T(Q)/100+.5)/10
175 E=INT(B(J-1)*T(J-1)/100000+.5)/10
180 A=INT(Y*I1*10+.5)/10
185 L=INT(Z*A+.5)
190 R=INT(Y*K*10+.5)/10
195 B=INT(Z*R+.5)
200 C=H(0)*X/1000
240 PRINT \PRINT
245 PRINT " (EMU/CC)      (G)      (EMU/CC)    (G)        (KOE)   (MG OE)   (KE
 250 PRINT "M/IN    M(S)    J(S)        M(R)      B(R)      H(CI)    (BH)MAX
 260 PRINT Y;TAB(8);A;TAB(15);L;TAB(24);R;TAB(33);B;
270 PRINT TAB(42);C;TAB(51);E;TAB(60);M
300 REM IN ON FE STD, VOL,SAT,REM,H(CI),DEMAG,X/IN
310 DATA
999 END
```

FLOW CHART FOR EASY AXIS DATA PROGRAM

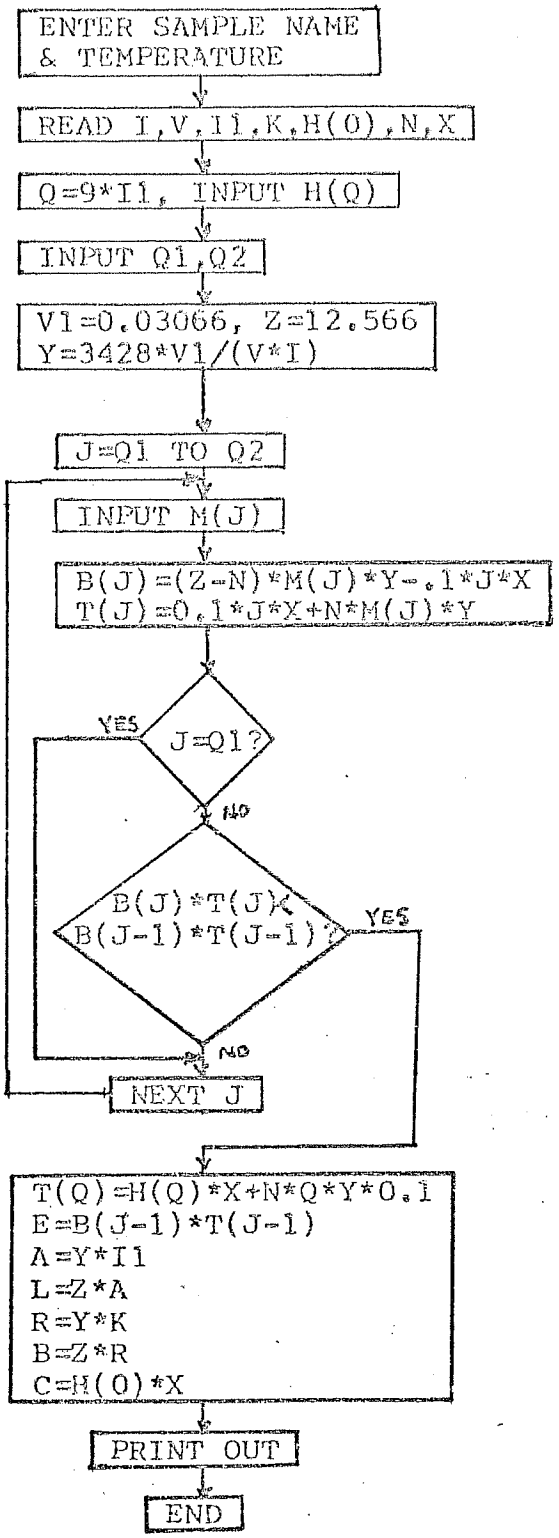

COMMENTS

I=INCHES BETWEEN $\pm M_s$ ON Fe STANDARD
V=VOLUME OF SAMPLE
I1=INCHES TO M_s
K=INCHES TO M_r
H(0)=INCHES TO H_{ci}
N=DEMAGNETIZING FACTOR=N_d
X=Oe/IN ON RECORDER
Q=Y COORDINATE OF H_K
H(Q)=INCHES TO H_K
Q1,Q2=LIMITS OF SWEEP TO FIND (BH)MAX
V1=VOLUME OF Fe STANDARD
$Z=4\pi$
Y=Y AXIS CALIBRATION
$B(J)=B=(4\pi-N_d)M+H$
T(J)=H

$T(Q)=H_K$
E=(BH)MAX
$A=M_s$
$L=4\pi M_s$
$R=M_r$
$B=B_r$
$C=H_{ci}$

Difficulty was encountered in saturating the samples at low temperatures due to the increased anisotropy. Saturation magnetization at low temperatures was measured by first saturating the sample at room temperature in an applied field of 100 kOe and then cooling the sample to 77 K while still in the magnetic field. There was no measurable change in saturation magnetization between 77 and 4.2 K.

C. Hard Axis Measurements

The hard axis magnetization curves were expected to yield the anisotropy field, H_A, and thus the anisotropy constant K_1 (K_2 is generally accepted as being very small for $SmCo_5$) directly. It was expected that the magnetization curves would be straight lines similar to the results of Benz and Martin[3] shown in figure 4. It was observed that the hard axis curves were loops and not straight lines. To find K_1 from these curves, it was necessary to calculate the magnetization curve for sintered magnets which is described in the next section.

D. Calculation of Magnetization Curves

The purpose of this calculation is to derive the decreasing field portion of parallel and perpendicular magnetization curves for an aligned compact of single-domain particles. The model assumes that the magnetization changes only by rotation. This type of behavior is found in the decreasing field portion of magnetization curves, especially in high fields.

The hard axis M vs H curve for a single crystal or an assembly of single crystals is given by Cullity[13] as,

$$H=2K_1/M_s(M/M_s)+4K_2/M_s(M/M_s)^3, \qquad (1)$$

where K_1 and K_2 are the anisotropy constants for a hexagonal crystal and are related to the anisotropy energy by,

$$E_k=K_1\sin^2\gamma+K_2\sin^4\gamma, \qquad (2)$$

where γ is defined as the angle between the saturation magnetization, M_s, and the c axis. The shape of the M/M_s vs H/H_A (H_A is the anisotropy field defined as the field at which a sample reaches saturation when the field is applied perpendicular to the easy axis) curve is shown in figure 5 for three cases, $K_2=0$, $K_2/K_1<0$ and $K_2/K_1>0$. If an assembly of particles is not perfectly aligned, the magnetization curve shows hysteresis and has a remanence due to the misorientation of the particles, as shown in figure 6.

To derive the hard axis magnetization curve, the following assumptions are made:

1. The sample is made up of a large number of noninteracting single-domain particles that have approximately the same magnetic moment;
2. The magnetization changes only by rotation in each particle;
3. The demagnetizing correction is small.

The coordinate system to be used for the calculation is defined in figure 7: $\hat{z}$=the axis of orientation, which is the easy axis of the sample; $\vec{P}=[\sin\phi\cos\theta,\sin\phi\sin\theta,\cos\phi]$=the easy axis of an individual particle; λ=the angle between $\vec{P}$ and $\hat{x}$. Using these definitions, λ can be found in terms of ϕ and θ from the dot product,

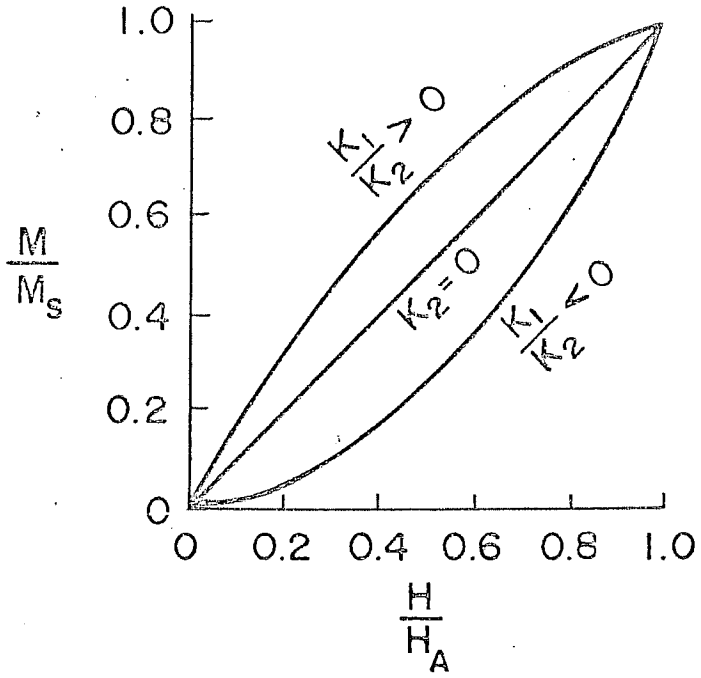

Figure 5. M/M_s vs H/H_A.

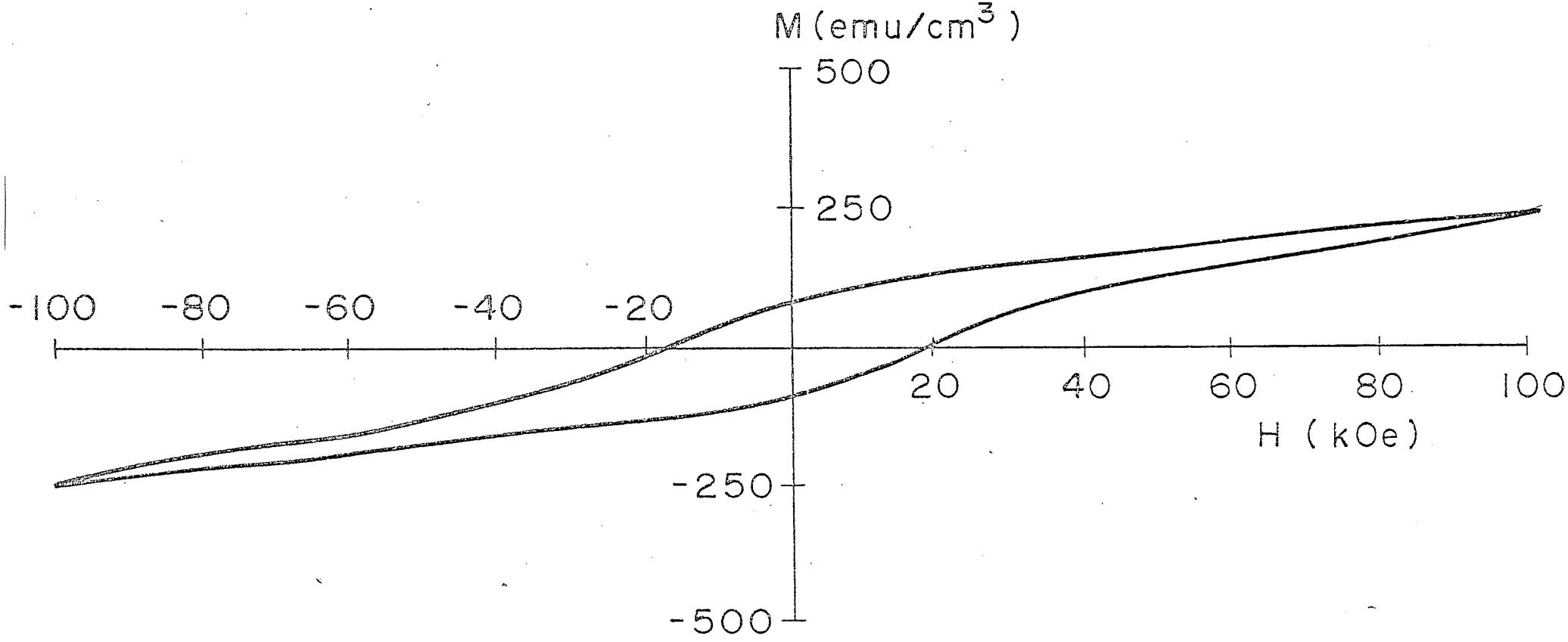

Figure 6. Observed hard axis magnetization curve for sintered $SmCo_5$. The sample was measured at 4.2 K and contains 17.08 atomic percent samarium.

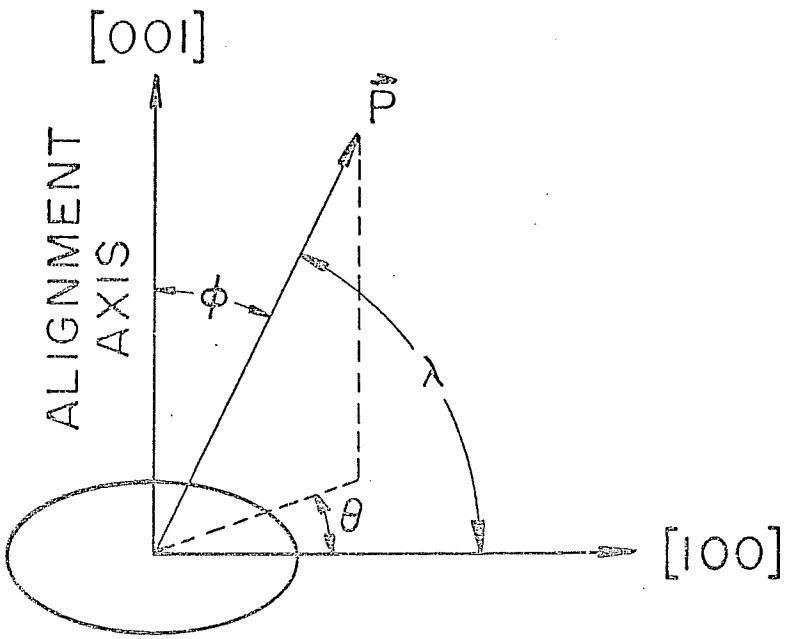

Figure 7. Coordinate system.

$$\cos\lambda=[\sin\phi\cos\theta,\sin\phi\sin\theta,\cos\phi]\cdot[\cos0^\circ,\cos90^\circ,\cos90^\circ]=\sin\phi\cos\theta. \quad (3)$$

The distribution of particle easy axes is assumed to be normal in terms of ϕ and uniformly distributed in θ. In spherical coordinates, the distribution is of the form,

$$f(\phi,\theta)dA=k\exp(-\phi^2/\beta^2)\sin\phi d\phi d\theta \quad (4)$$

where $dA=\sin\phi d\phi d\theta$, is an element of spherical area. This describes a distribution with a maximum at $\phi=0$, decreasing exponentially with ϕ as ϕ departs from 0 in any direction from the axis of orientation. The quantity β describes the rapidity of the drop; a large β means a slow drop or a broad distribution. Therefore, β measures the degree of particle misorientation. The function $f(\phi,\theta)$ is defined for the region $0\leq\phi\leq\pi/2$ and $0\leq\theta\leq2\pi$. The normalization constant, k, is determined by the condition,

$$\int_A f(\phi,\theta)dA=1. \quad (5)$$

If $\beta\ll\pi/2$, the upper limit of $\pi/2$ on ϕ can be replaced by infinity. Then the integral and any integral of the form,

$$I(m)=\int_0^{2\pi}\int_0^{\infty} f(\phi,\theta)\ \phi^m\ \sin\phi d\phi d\theta, \quad m=\text{integer} \quad (6)$$

can be evaluated by expanding $\sin\phi$ as a Taylor series:

$$\sin\phi=\sum_{n=1}^{\infty}(-1)^{n-1}\phi^{2n-1}/(2n-1)!. \quad (7)$$

Equation (7) can be substituted into (6), the θ integration can be performed, and the operations of integration and summation can be reversed to yield,

$$I(m)=2\pi k\sum_{n=1}^{\infty}\frac{(-1)^{n-1}}{(2n-1)!}\int_{o}^{\infty}\exp(-\phi^2/\beta^2)\ \phi^{2n+m-2}\ \phi d\phi. \qquad (8)$$

The integral can be solved by substitution by letting $x=\phi^2/\beta^2$ so that $\phi d\phi=\beta^2 dx/2$. The integral then becomes,

$$I(m)=\pi k\sum_{n=1}^{\infty}\frac{(-1)^{n-1}\beta^{2n+m}}{(2n-1)!}\int_{o}^{\infty}\exp(-x)\ x^{n-1+m/2}\ dx. \qquad (9)$$

The integral is a gamma function, specifically $\Gamma(n+m/2)$, so that,

$$I(m)=\pi k\sum_{n=1}^{\infty}\frac{(-1)^{n-1}\beta^{2n+m}\Gamma(n+m/2)}{(2n-1)!}. \qquad (10)$$

The normalization condition expressed in (5) can now be written as,

$$I(0)=\pi k\sum_{n=1}^{\infty}(-1)^{n-1}\beta^{2n}\Gamma(n)/(2n-1)!=1, \qquad (11)$$

so that k can be expressed as a series;

$$k=1/\pi(\beta^2-\beta^4/6+\beta^6/60-\beta^8/840+\ \ldots). \qquad (12)$$

The result in (11) was originally given by Legendre,[14] using a different method. For our calculation, the first four terms of the series will be used. Clearly, I(1) and I(2) represent the first and second moments of $f(\phi,\theta)$ for ϕ. Therefore, the mean, μ, and variance, σ^2, are given by I(1) and $I(2)-I(1)^2$ respectively. We have:

$$I(1)=\mu=\pi k\sum_{n=1}^{\infty}(-1)^{n-1}\beta^{2n-1}\Gamma(n+\tfrac{1}{2})/(2n-1)! \qquad (13)$$

$$=\frac{\sqrt{\pi}\beta(1-\beta^2/4+\beta^4/32-\beta^6/384+\ \ldots)}{2(1-\beta^2/6+\beta^4/60-\beta^6/840+\ \ldots)}$$

$$\sigma^2 = I(2) - I(1)^2 = \frac{\beta^2(1-\beta^2/3+\beta^4/20-\beta^6/210+\ldots)}{(1-\beta^2/6+\beta^4/60-\beta^6/840+\ldots)} \qquad (14)$$

$$- \frac{\pi\beta^2(1-\beta^2/4+\beta^4/32-\beta^6/384+\ldots)^2}{4(1-\beta^2/6+\beta^4/60-\beta^6/840+\ldots)^2}.$$

For small β, $\mu = \sqrt{\pi}\beta/2$ and $\sigma^2 = \beta^2(1-\pi/4)$. This agrees with the results obtained for a Rayleigh distribution,[15] which describes a normal distribution about a point in a plane, as opposed to the case treated here which is a distribution about a point on the surface of a sphere.

To calculate the magnetization of an assembly of single-domain particles whose distribution about an alignment axis is given by (4), we consider the torque exerted by an applied field $\vec{H}$ on the particles whose orientation is in an element of spherical area dA. This torque is exactly balanced by the crystal anisotropy torque acting to hold the magnetization along the local easy axis $\vec{P}$. Thus,

$$\vec{H} \times \vec{M}_s = dE_K/d\gamma \qquad (15)$$

where γ is defined in figure 8a for the case when H is applied perpendicular to the alignment axis and in figure 8b for the case when H is applied parallel to the alignment axis. Since $E_K = K_1\sin^2\gamma + K_2\sin^4\gamma$ for a hexagonal crystal, equation (15) can be expressed as,

$$HM_s\sin(\lambda-\gamma) = K_1\sin 2\gamma + 2K_2\sin 2\gamma\sin^2\gamma = K_1\sin 2\gamma\left(1+\frac{2K_2}{K_1}\sin^2\gamma\right) \qquad (16)$$

for the perpendicular field case and,

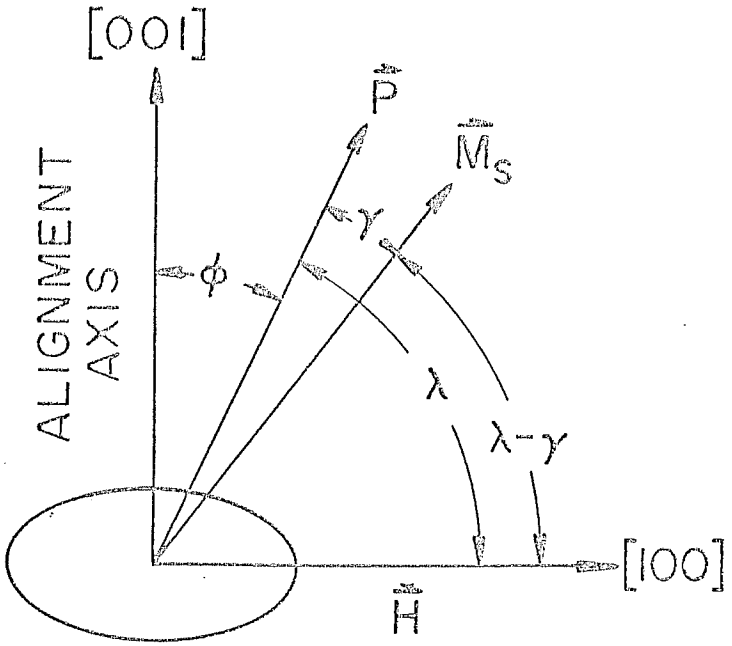

Figure 8a. Definition of angles for hard axis case.

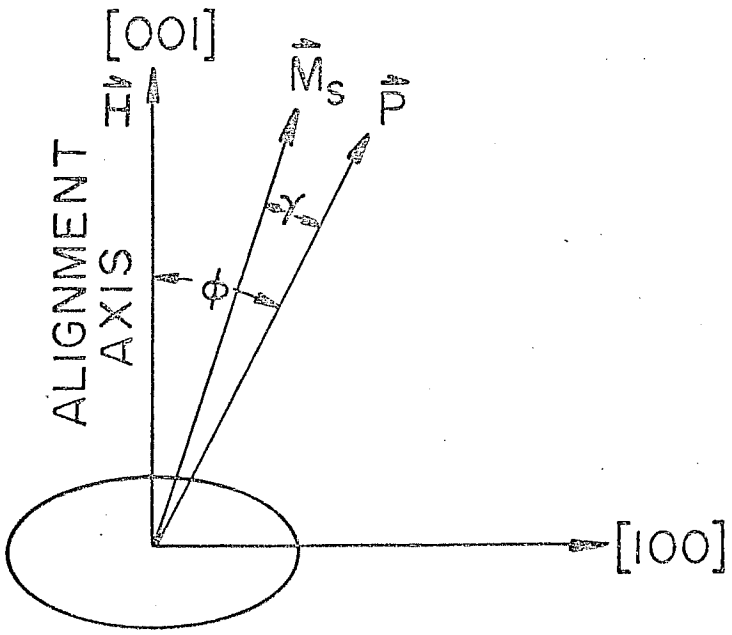

Figure 8b. Definition of angles for easy axis case.

$$HM_s\sin(\phi-\gamma)=K_1\sin 2\gamma+2K_2\sin 2\gamma\sin^2\gamma=K_1\sin 2\gamma\left(1+\frac{2K}{K_1}2\ \sin^2\gamma\right) \qquad (17)$$

for the parallel field case. For any combination of H, ϕ, θ, K_1, and K_2/K_1, equations (16) or (17) can be used to determine γ for the particles whose orientation is in dA.

To obtain the resultant magnetization of the entire sample, it is necessary to sum the individual contributions of each unit area dA. Thus, $M_\perp/M_s$ can be found by evaluating the integral,

$$M_\perp/M_s=\int_0^\infty\int_0^{2\pi}\cos(\lambda-\gamma)f(\phi,\theta)\sin\phi d\theta d\phi. \qquad (18)$$

Similarly, $M_\parallel/M_s$ is given by,

$$M_\parallel/M_s=\int_0^\infty\int_0^{2\pi}\cos(\phi-\gamma)f(\phi,\theta)\sin\phi d\theta d\phi. \qquad (19)$$

In practice, the integrals (18) and (19) can be solved using the computer to generate $M_\perp/M_s$ or $M_\parallel/M_s$ vs h ($=HM_s/(2K_1+4K_2)$) curves, for selected values of β. The results of calculations based on (18) are given in table 2 for some different values of K_2/K_1. Table 3 gives the results of calculations based on (19) for the special case when H=0, γ=0, for which $M_\parallel/M_s=M_r/M_s$, the ratio of remanence to saturation, or remanence ratio (sometimes called the alignment factor).

1. Comparison of the assumed particle distribution to a measured particle distribution

D. L. Martin has reported a method of metallographic analysis to determine the texture of $SmCo_5$.[2] On heat treating a sintered sample for 10 days at 1025 K, $SmCo_5$ undergoes a

PROGRAM 2

```
0001                    DIMENSION A(10)
0002                    Z=0.0
0003                    W=0.5
0004                    DO 900 I=1,21
0005                     H=(I-1)*.2
0006                    DO 800 J=1,9
0007                    B=J*.05
0008                    D=.0157/(3.14159*(B-B**3/6+B**5/60-B**7/840))
0009                    SUMM=0.0
0010                    X=.05*B
0011          500       C=D*EXP(-(X/B)*(X/B))*SIN(X)
0012                    SUMN=0.0
0013                    DO 700 L=157,2983,314
0014                     Y=(3140-L)*.0005
0015                    R=ARCOS(COS(Y)*SIN(X))
0016                    IF (I.EQ.1) GOTO 700
0017                    Z=R
0018          625       Z=Z-.1
0019                    IF((1+2.0*W*SIN(Z)*SIN(Z))*SIN(2*Z) -H*SIN(R-Z))   650,700,625
0020          650       Z=Z+.01
0021                    IF((1+2.0*W*SIN(Z)*SIN(Z))*SIN(2*Z) -H*SIN(R-Z))   650,700,675
0022          675       Z=Z-.001
0023                    IF((1+2.0*W*SIN(Z)*SIN(Z))*SIN(2*Z) -H*SIN(R-Z))   700,700,675
0024          700       SUMN=SUMN+COS(R-Z)
0025                    SUMM=SUMM+SUMN*C
0026                    F=.0005-SUMN*C/SUMM
0027                    IF (F.GT.0) GOTO 800
0028          750       X=X+(.1*B)
0029                    GOTO 500
0030          800       A(J)=SUMM*4.0
0031                    H1=(I-1)*.1
0032          830       WRITE (6,850) H1,A(1),A(2),A(3),A(4),A(5),A(6),A(7),A(8),A(9)
0033          850       FORMAT (F10.1,9F10.4)
0034          900       CONTINUE
0035                    STOP
0036                    END
```

TABLE 2

h vs m for β=0.05 to 0.45

for $K_2=K_1$, $K_2=0.5K_1$, $K_2=0.1K_1$, $K_2=0$, $K_2=-0.1K_1$, and $K_2=-0.5K_1$.

$K_2=K_1$

h	β=0.05	β=0.10	β=0.15	β=0.20	β=0.25	β=0.30	β=0.35	β=0.40	β=0.45
0.0	0.0282	0.0563	0.0841	0.1114	0.1382	0.1644	0.1898	0.2143	0.2378
0.1	0.1253	0.1526	0.1795	0.2057	0.2312	0.2559	0.2797	0.3025	0.3244
0.2	0.2130	0.2391	0.2646	0.2893	0.3132	0.3362	0.3584	0.3795	0.3996
0.3	0.2882	0.3129	0.3369	0.3601	0.3824	0.4039	0.4244	0.4439	0.4624
0.4	0.3523	0.3756	0.3981	0.4198	0.4407	0.4606	0.4796	0.4977	0.5148
0.5	0.4075	0.4295	0.4505	0.4709	0.4903	0.5089	0.5265	0.5433	0.5591
0.6	0.4559	0.4765	0.4961	0.5152	0.5333	0.5506	0.5670	0.5825	0.5972
0.7	0.4989	0.5181	0.5366	0.5543	0.5712	0.5873	0.6025	0.6169	0.6303
0.8	0.5376	0.5555	0.5727	0.5892	0.6049	0.6199	0.6340	0.6474	0.6598
0.9	0.5727	0.5894	0.6054	0.6207	0.6352	0.6491	0.6623	0.6745	0.6862
1.0	0.6050	0.6205	0.6352	0.6493	0.6628	0.6757	0.6878	0.6991	0.7100
1.1	0.6349	0.6491	0.6626	0.6756	0.6881	0.6999	0.7109	0.7216	0.7316
1.2	0.6627	0.6757	0.6880	0.6999	0.7113	0.7220	0.7323	0.7422	0.7514
1.3	0.6887	0.7002	0.7115	0.7224	0.7325	0.7425	0.7520	0.7611	0.7696
1.4	0.7132	0.7233	0.7333	0.7431	0.7525	0.7616	0.7703	0.7786	0.7864
1.5	0.7362	0.7453	0.7539	0.7626	0.7711	0.7793	0.7872	0.7948	0.8020
1.6	0.7580	0.7655	0.7732	0.7809	0.7885	0.7958	0.8030	0.8099	0.8165
1.7	0.7787	0.7849	0.7914	0.7980	0.8048	0.8113	0.8178	0.8240	0.8299
1.8	0.7983	0.8031	0.8085	0.8142	0.8200	0.8258	0.8316	0.8372	0.8425
1.9	0.8170	0.8205	0.8247	0.8294	0.8344	0.8394	0.8445	0.8495	0.8543
2.0	0.8349	0.8369	0.8400	0.8438	0.8479	0.8522	0.8566	0.8610	0.8653

$K_2 = 0.5K_1$

h	β=0.05	β=0.10	β=0.15	β=0.20	β=0.25	β=0.30	β=0.35	β=0.40	β=0.45
0.0	0.0282	0.0563	0.0841	0.1114	0.1382	0.1644	0.1898	0.2143	0.2378
0.1	0.1262	0.1535	0.1803	0.2065	0.2320	0.2567	0.2805	0.3033	0.3251
0.2	0.2188	0.2446	0.2700	0.2945	0.3182	0.3411	0.3630	0.3839	0.4039
0.3	0.3027	0.3269	0.3503	0.3730	0.3948	0.4158	0.4358	0.4548	0.4728
0.4	0.3776	0.3999	0.4214	0.4421	0.4620	0.4810	0.4992	0.5163	0.5326
0.5	0.4444	0.4646	0.4841	0.5029	0.5208	0.5380	0.5543	0.5698	0.5845
0.6	0.5039	0.5221	0.5397	0.5566	0.5727	0.5881	0.6027	0.6166	0.6296
0.7	0.5574	0.5738	0.5893	0.6043	0.6187	0.6324	0.6454	0.6577	0.6694
0.8	0.6061	0.6203	0.6340	0.6471	0.6598	0.6719	0.6833	0.6942	0.7047
0.9	0.6506	0.6627	0.6745	0.6858	0.6968	0.7072	0.7173	0.7270	0.7361
1.0	0.6915	0.7013	0.7110	0.7206	0.7300	0.7391	0.7479	0.7563	0.7644
1.1	0.7292	0.7368	0.7446	0.7525	0.7604	0.7681	0.7756	0.7828	0.7898
1.2	0.7642	0.7696	0.7755	0.7817	0.7881	0.7944	0.8007	0.8069	0.8128
1.3	0.7968	0.7999	0.8039	0.8084	0.8133	0.8184	0.8235	0.8287	0.8337
1.4	0.8272	0.8279	0.8299	0.8329	0.8364	0.8403	0.8443	0.8484	0.8526
1.5	0.8555	0.8537	0.8539	0.8553	0.8575	0.8601	0.8632	0.8664	0.8698
1.6	0.8818	0.8776	0.8759	0.8758	0.8767	0.8783	0.8803	0.8827	0.8853
1.7	0.9062	0.8994	0.8959	0.8944	0.8941	0.8947	0.8959	0.8975	0.8994
1.8	0.9284	0.9192	0.9140	0.9111	0.9098	0.9094	0.9098	0.9108	0.9120
1.9	0.9483	0.9368	0.9300	0.9260	0.9237	0.9226	0.9222	0.9225	0.9232
2.0	0.9650	0.9517	0.9438	0.9388	0.9358	0.9340	0.9331	0.9329	0.9331

$K_2=0.1K_2$

h	β=0.05	β=0.10	β=0.15	β=0.20	β=0.25	β=0.30	β=0.35	β=0.40	β=0.45
0.0	0.0282	0.0563	0.0841	0.1114	0.1382	0.1644	0.1898	0.2143	0.2378
0.1	0.1269	0.1542	0.1811	0.2072	0.2327	0.2574	0.2812	0.3039	0.3257
0.2	0.2242	0.2500	0.2751	0.2994	0.3229	0.3456	0.3674	0.3881	0.4079
0.3	0.3185	0.3420	0.3649	0.3869	0.4081	0.4284	0.4478	0.4663	0.4839
0.4	0.4092	0.4298	0.4498	0.4690	0.4876	0.5053	0.5222	0.5383	0.5535
0.5	0.4955	0.5128	0.5295	0.5457	0.5613	0.5762	0.5905	0.6041	0.6169
0.6	0.5770	0.5906	0.6037	0.6166	0.6291	0.6412	0.6528	0.6638	0.6745
0.7	0.6540	0.6630	0.6724	0.6818	0.6911	0.7001	0.7091	0.7179	0.7264
0.8	0.7260	0.7301	0.7352	0.7410	0.7471	0.7535	0.7600	0.7665	0.7729
0.9	0.7930	0.7917	0.7925	0.7946	0.7976	0.8013	0.8054	0.8097	0.8141
1.0	0.8544	0.8473	0.8437	0.8423	0.8424	0.8435	0.8453	0.8476	0.8502
1.1	0.9092	0.8960	0.8882	0.8836	0.8810	0.8798	0.8796	0.8802	0.8813
1.2	0.9538	0.9356	0.9245	0.9173	0.9126	0.9096	0.9079	0.9071	0.9069
1.3	0.9779	0.9607	0.9491	0.9411	0.9355	0.9316	0.9290	0.9274	0.9265
1.4	0.9881	0.9745	0.9642	0.9566	0.9509	0.9469	0.9440	0.9420	0.9408
1.5	0.9928	0.9826	0.9738	0.9670	0.9617	0.9578	0.9549	0.9528	0.9513
1.6	0.9952	0.9875	0.9803	0.9742	0.9695	0.9657	0.9629	0.9609	0.9594
1.7	0.9966	0.9907	0.9847	0.9794	0.9752	0.9718	0.9691	0.9671	0.9656
1.8	0.9974	0.9928	0.9878	0.9833	0.9795	0.9763	0.9739	0.9720	0.9706
1.9	0.9980	0.9943	0.9901	0.9861	0.9828	0.9799	0.9777	0.9759	0.9745
2.0	0.9983	0.9953	0.9918	0.9884	0.9853	0.9828	0.9807	0.9791	0.9778

$K_2=0$

h	β=0.05	β=0.10	β=0.15	β=0.20	β=0.25	β=0.30	β=0.35	β=0.40	β=0.45
0.0	0.0282	0.0563	0.0841	0.1114	0.1382	0.1644	0.1898	0.2143	0.2378
0.1	0.1271	0.1544	0.1812	0.2074	0.2329	0.2575	0.2813	0.3040	0.3259
0.2	0.2257	0.2514	0.2764	0.3007	0.3242	0.3469	0.3685	0.3893	0.4090
0.3	0.3234	0.3467	0.3693	0.3911	0.4121	0.4322	0.4514	0.4697	0.4872
0.4	0.4201	0.4402	0.4595	0.4782	0.4962	0.5134	0.5299	0.5456	0.5605
0.5	0.5157	0.5315	0.5469	0.5619	0.5764	0.5904	0.6038	0.6167	0.6288
0.6	0.6096	0.6203	0.6310	0.6417	0.6524	0.6628	0.6729	0.6828	0.6923
0.7	0.7015	0.7055	0.7108	0.7168	0.7232	0.7300	0.7370	0.7439	0.7508
0.8	0.7904	0.7866	0.7856	0.7865	0.7887	0.7917	0.7953	0.7993	0.8036
0.9	0.8739	0.8608	0.8533	0.8491	0.8470	0.8464	0.8469	0.8482	0.8501
1.0	0.9444	0.9228	0.9096	0.9010	0.8954	0.8919	0.8898	0.8889	0.8887
1.1	0.9783	0.9587	0.9451	0.9354	0.9285	0.9236	0.9203	0.9181	0.9169
1.2	0.9897	0.9758	0.9643	0.9555	0.9488	0.9439	0.9403	0.9377	0.9360
1.3	0.9942	0.9846	0.9755	0.9680	0.9620	0.9573	0.9538	0.9512	0.9493
1.4	0.9963	0.9895	0.9824	0.9761	0.9709	0.9667	0.9634	0.9609	0.9590
1.5	0.9974	0.9924	0.9868	0.9816	0.9771	0.9734	0.9704	0.9680	0.9662
1.6	0.9980	0.9942	0.9898	0.9854	0.9815	0.9783	0.9756	0.9734	0.9717
1.7	0.9984	0.9955	0.9919	0.9882	0.9849	0.9819	0.9795	0.9776	0.9760
1.8	0.9987	0.9964	0.9934	0.9903	0.9874	0.9848	0.9826	0.9808	0.9794
1.9	0.9989	0.9970	0.9945	0.9918	0.9893	0.9870	0.9851	0.9835	0.9821
2.0	0.9990	0.9975	0.9953	0.9930	0.9908	0.9888	0.9870	0.9856	0.9844

$K_2 = -0.1K_1$

h	β=0.05	β=0.10	β=0.15	β=0.20	β=0.25	β=0.30	β=0.35	β=0.40	β=0.45
0.0	0.0282	0.0563	0.0841	0.1114	0.1382	0.1644	0.1898	0.2143	0.2378
0.1	0.1273	0.1546	0.1814	0.2076	0.2331	0.2577	0.2814	0.3042	0.3260
0.2	0.2273	0.2530	0.2779	0.3022	0.3256	0.3482	0.3698	0.3905	0.4102
0.3	0.3289	0.3519	0.3742	0.3958	0.4165	0.4364	0.4554	0.4735	0.4908
0.4	0.4334	0.4525	0.4711	0.4891	0.5064	0.5230	0.5389	0.5541	0.5685
0.5	0.5425	0.5561	0.5696	0.5828	0.5958	0.6085	0.6207	0.6326	0.6437
0.6	0.6589	0.6639	0.6702	0.6773	0.6849	0.6928	0.7008	0.7089	0.7167
0.7	0.7855	0.7772	0.7735	0.7727	0.7737	0.7760	0.7792	0.7830	0.7871
0.8	0.9193	0.8910	0.8746	0.8644	0.8580	0.8543	0.8524	0.8518	0.8522
0.9	0.9785	0.9543	0.9365	0.9237	0.9146	0.9082	0.9037	0.9008	0.8991
1.0	0.9916	0.9773	0.9640	0.9531	0.9447	0.9382	0.9334	0.9299	0.9274
1.1	0.9956	0.9870	0.9776	0.9691	0.9619	0.9562	0.9517	0.9482	0.9457
1.2	0.9973	0.9917	0.9849	0.9783	0.9725	0.9676	0.9636	0.9604	0.9580
1.3	0.9981	0.9942	0.9892	0.9841	0.9794	0.9752	0.9717	0.9689	0.9667
1.4	0.9986	0.9957	0.9919	0.9879	0.9840	0.9805	0.9775	0.9750	0.9729
1.5	0.9988	0.9967	0.9937	0.9905	0.9872	0.9843	0.9817	0.9795	0.9777
1.6	0.9990	0.9974	0.9950	0.9923	0.9896	0.9871	0.9848	0.9829	0.9812
1.7	0.9992	0.9978	0.9959	0.9936	0.9913	0.9892	0.9872	0.9855	0.9840
1.8	0.9993	0.9982	0.9965	0.9947	0.9927	0.9908	0.9891	0.9876	0.9863
1.9	0.9993	0.9984	0.9971	0.9954	0.9937	0.9921	0.9906	0.9892	0.9880
2.0	0.9994	0.9986	0.9974	0.9961	0.9946	0.9931	0.9918	0.9906	0.9895

$K_2 = -0.5K_1$

h	β=0.05	β=0.10	β=0.15	β=0.20	β=0.25	β=0.30	β=0.35	β=0.40	β=0.45
0.0	0.0282	0.0563	0.0841	0.1114	0.1382	0.1644	0.1898	0.2143	0.2378
0.1	0.9992	0.9305	0.8046	0.7125	0.6587	0.6195	0.5948	0.5866	0.5790
0.2	0.9997	0.9925	0.9455	0.8818	0.8227	0.7865	0.7634	0.7425	0.7286
0.3	0.9997	0.9989	0.9826	0.9458	0.9093	0.8751	0.8468	0.8364	0.8227
0.4	0.9997	0.9996	0.9954	0.9778	0.9545	0.9309	0.9146	0.8982	0.8845
0.5	0.9997	0.9997	0.9987	0.9926	0.9799	0.9655	0.9528	0.9407	0.9314
0.6	0.9997	0.9997	0.9995	0.9979	0.9931	0.9862	0.9778	0.9704	0.9630
0.7	0.9997	0.9997	0.9996	0.9991	0.9973	0.9939	0.9895	0.9847	0.9800
0.8	0.9997	0.9997	0.9996	0.9994	0.9985	0.9967	0.9940	0.9909	0.9877
0.9	0.9997	0.9997	0.9997	0.9995	0.9990	0.9979	0.9962	0.9941	0.9918
1.0	0.9997	0.9997	0.9997	0.9996	0.9993	0.9985	0.9973	0.9958	0.9942
1.1	0.9997	0.9997	0.9997	0.9996	0.9994	0.9989	0.9980	0.9969	0.9956
1.2	0.9997	0.9997	0.9997	0.9996	0.9995	0.9991	0.9985	0.9976	0.9966
1.3	0.9997	0.9997	0.9997	0.9996	0.9995	0.9992	0.9988	0.9981	0.9973
1.4	0.9997	0.9997	0.9997	0.9997	0.9996	0.9993	0.9990	0.9984	0.9978
1.5	0.9997	0.9997	0.9997	0.9997	0.9996	0.9994	0.9991	0.9987	0.9981
1.6	0.9997	0.9997	0.9997	0.9997	0.9996	0.9995	0.9992	0.9989	0.9984
1.7	0.9997	0.9997	0.9997	0.9997	0.9996	0.9995	0.9993	0.9990	0.9986
1.8	0.9997	0.9997	0.9997	0.9997	0.9996	0.9995	0.9994	0.9991	0.9988
1.9	0.9997	0.9997	0.9997	0.9997	0.9996	0.9996	0.9994	0.9992	0.9989
2.0	0.9997	0.9997	0.9997	0.9997	0.9997	0.9996	0.9995	0.9993	0.9990

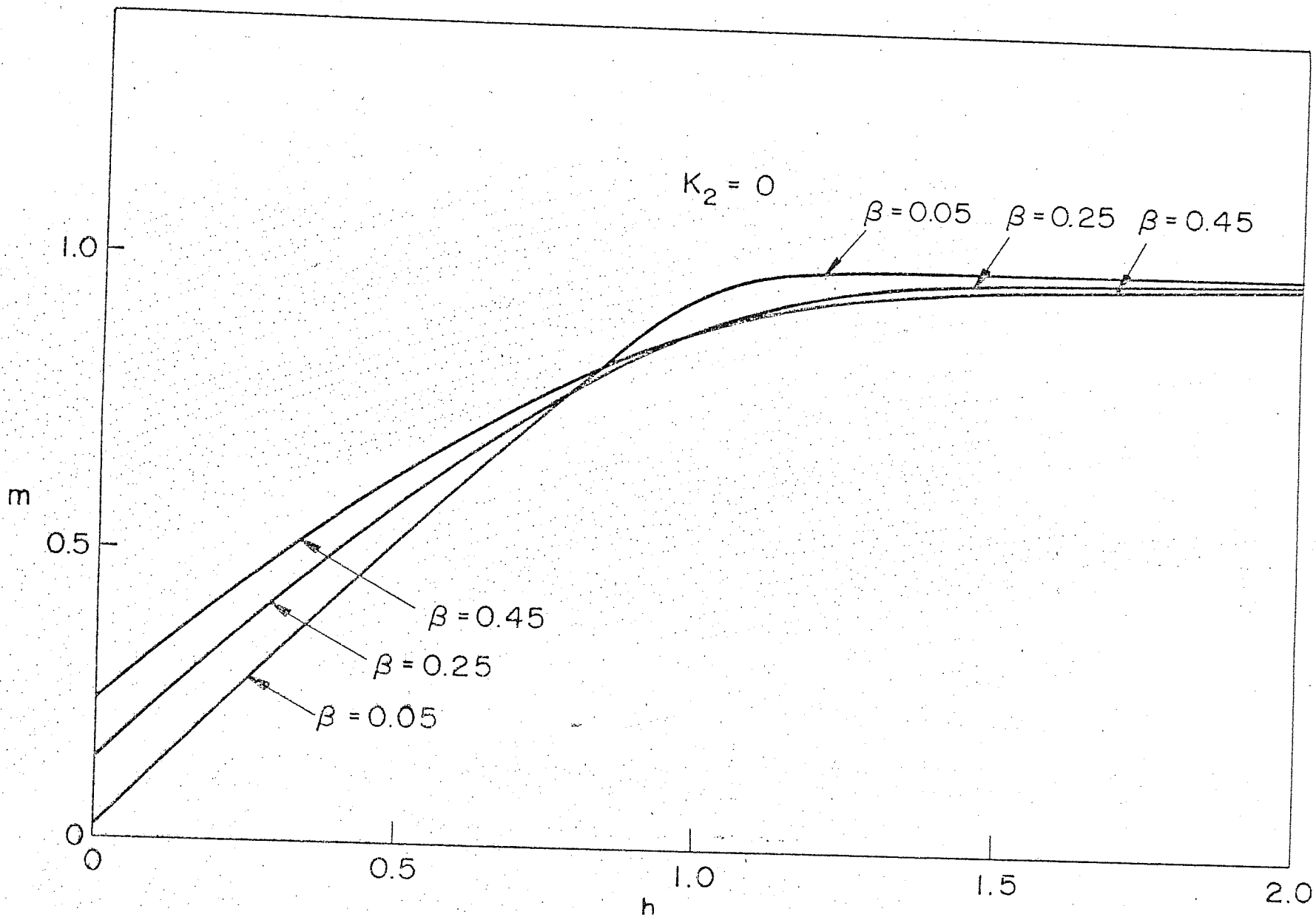
$K_2 = 0$
$\beta = 0.05$
$\beta = 0.25$
$\beta = 0.45$
$\beta = 0.45$
$\beta = 0.25$
$\beta = 0.05$
m
h
0
0.5
1.0
0
0.5
1.0
1.5
2.0

TABLE 3

B	M(R)/M(S)	VARIANCE	STD DEV
.05	.9984	5.400000E-04	.0232
.06	.9979	7.700000E-04	.0278
.07	.9972	1.050000E-03	.0324
.08	.9965	1.370000E-03	.037
.09	.9956	1.740000E-03	.0417
.1	.9947	2.140000E-03	.0463
.11	.9937	2.590000E-03	.0509
.12	.9925	3.080000E-03	.0555
.13	.9913	3.620000E-03	.0601
.14	.99	4.190000E-03	.0647
.15	.9886	4.810000E-03	.0694
.16	.9871	5.470000E-03	.074
.17	.9855	6.170000E-03	.0786
.18	.9838	6.920000E-03	.0832
.19	.982	7.700000E-03	.0878
.2	.9801	8.530000E-03	.0923
.21	.9781	9.390000E-03	.0969
.22	.976	.0103	.1015
.23	.9739	.01125	.1061
.24	.9716	.01224	.1106
.25	.9693	.01327	.1152
.26	.9668	.01434	.1198
.27	.9643	.01545	.1243
.28	.9617	.0166	.1289
.29	.9591	.01779	.1334
.3	.9563	.01902	.1379
.31	.9534	.02029	.1425
.32	.9505	.0216	.147
.33	.9472	.02294	.1515
.34	.9442	.02433	.156
.35	.941	.02575	.1605
.36	.9378	.02721	.165
.37	.9345	.02871	.1694
.38	.9311	.03024	.1739
.39	.9276	.03181	.1784
.4	.9241	.03342	.1828
.41	.9205	.03506	.1872
.42	.9168	.03674	.1917
.43	.9131	.03845	.1961
.44	.9093	.0402	.2005
.45	.9054	.04198	.2049

READY.

eutectoid decomposition, $SmCo_5 \rightarrow Sm_2Co_7 + Sm_2Co_{17}$. Lamellae precipitate preferentially on the basal plane of the hexagonal $SmCo_5$, as shown in Martin's micrograph, figure 9. A grid is placed over the micrograph, and an angle of misorientation ϕ' is measured at each point on the grid. Figure 10 shows a histogram of measured angles.

The angle ϕ', however, is not equal to the angle ϕ defined in figure 7. ϕ' is the projection of ϕ onto the plane of the metallographic section of the sample. The geometric relationship between ϕ' and ϕ is shown in figure 11. Mathematically, the relationship between ϕ' and ϕ is shown by the following argument:

If $\vec{P}$ and $\vec{P}'$ are taken to be unit vectors, their components in cartesian coordinates are,

$$\vec{P} = \left[\cos\theta\sin\phi, \sin\theta\sin\phi, \cos\phi\right] \text{ and}$$

$$\vec{P}' = \left[\sin\phi', 0, \cos\phi'\right] .$$

If α is defined as the angle between P and P', then

$$\cos\alpha = \vec{P}\cdot\vec{P}' = \cos\theta\sin\phi\sin\phi' + \cos\phi\cos\phi'.$$

The law of spherical angles gives,

$$\cos\phi = \cos\alpha\cos\phi' = \cos\theta\sin\phi\sin\phi'\cos\phi' + \cos\phi\cos^2\phi'.$$

Dividing by $\cos\phi$, we have,

$$1 = \cos\theta\tan\phi\sin\phi'\cos\phi' + \cos^2\phi',$$

$$\tan\phi' = \cos\theta\tan\phi. \qquad (20)$$

To determine if Martin's observed distribution agrees with the assumed distribution of equation (4), an assumed distribution obeying (4) for a fixed β can be converted to a predicted

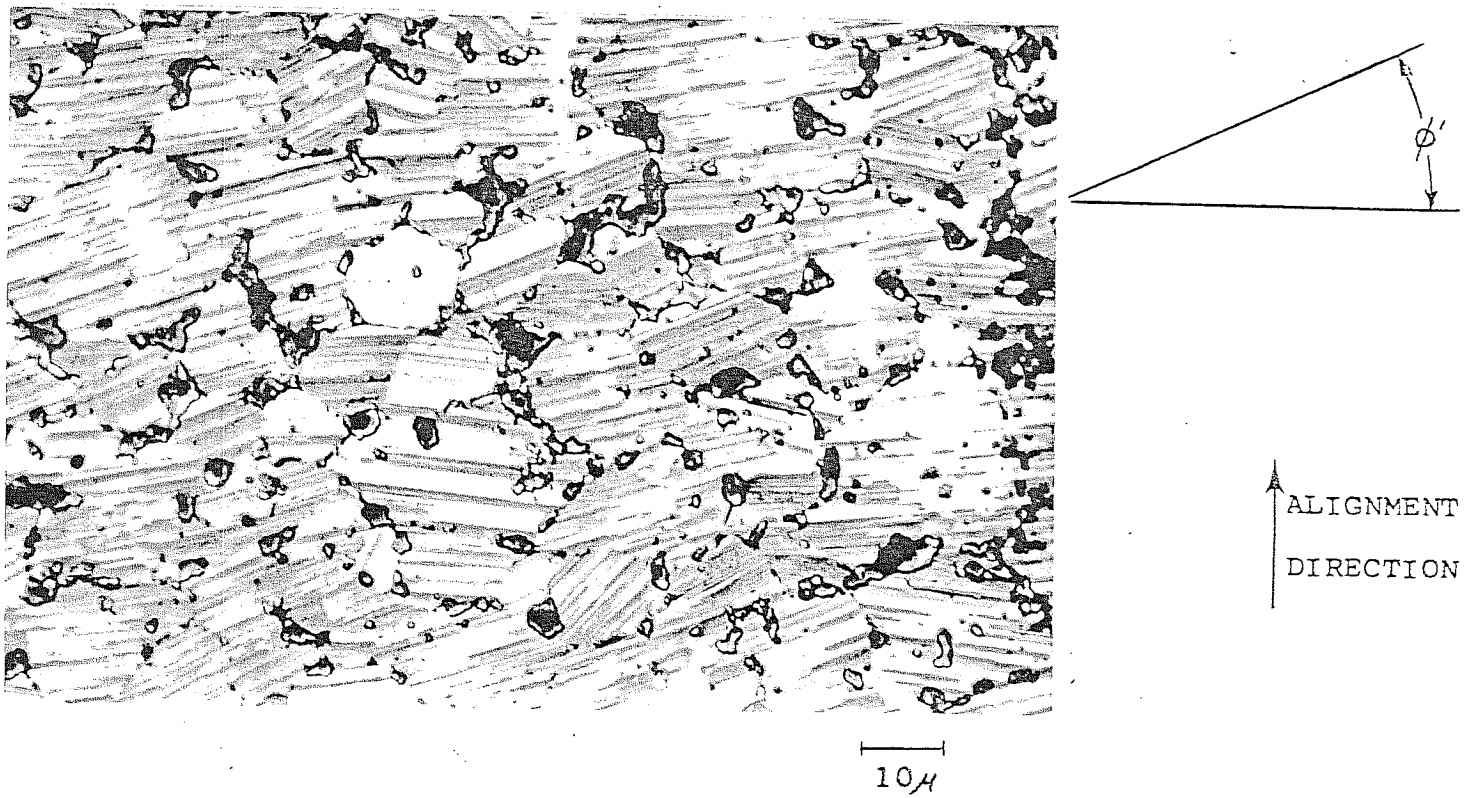

Figure 9. D. L. Martin's micrograph of aged sintered $SmCo_5$.[2]

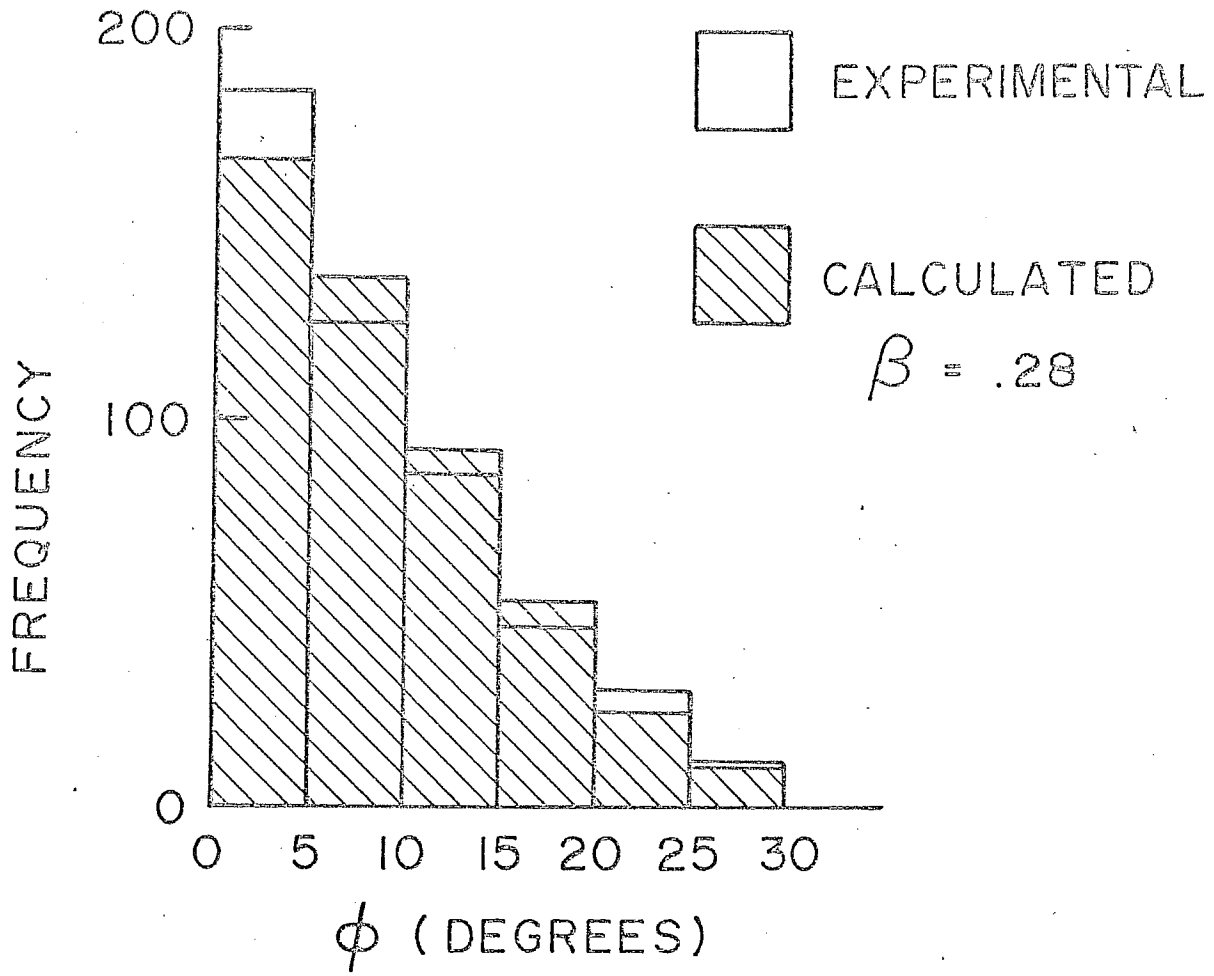

Figure 10. Calculated and experimental histograms.[2]

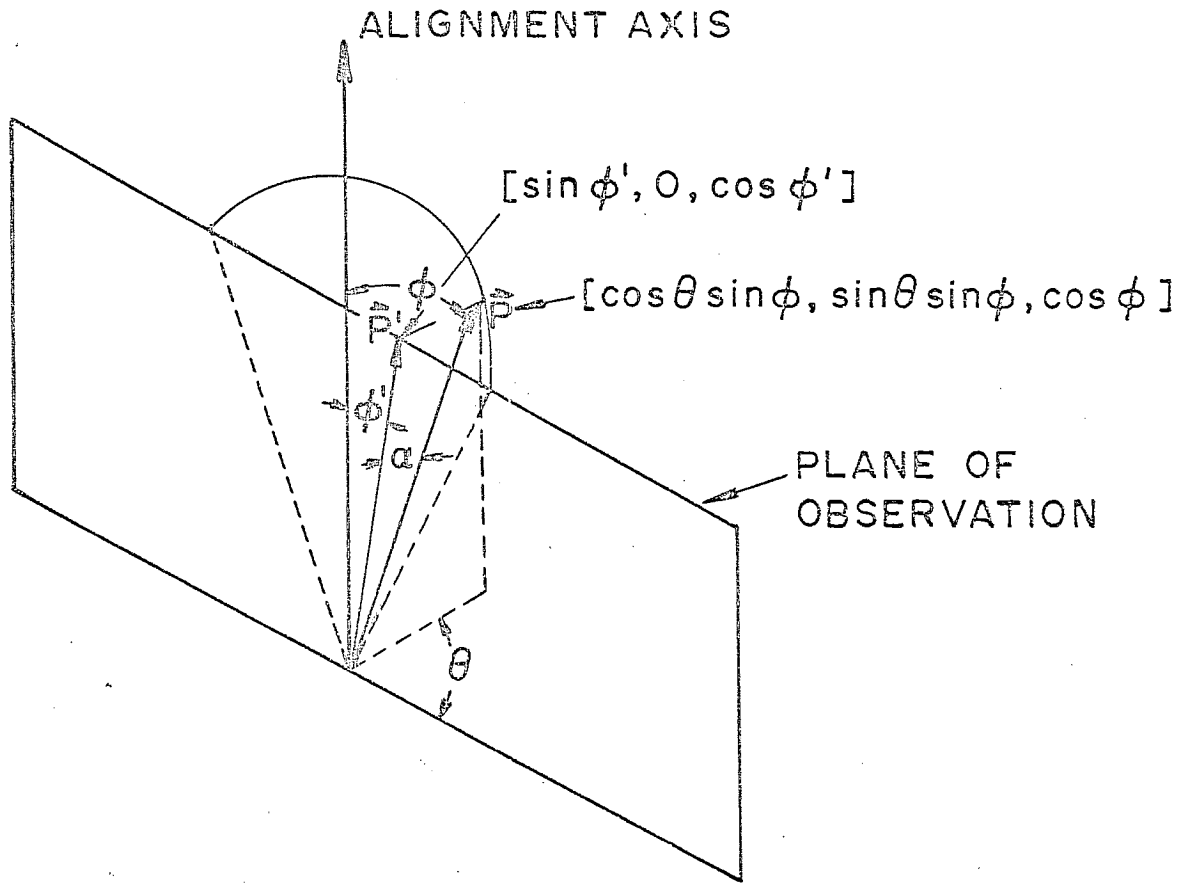

Figure 11. Relationship between Ø and Ø'.

projected two-dimensional distribution by using equation (20). The calculated histogram can then be compared to Martin's histogram. Figure 10 shows a histogram calculated for $\beta = 0.28$ superimposed on Martin's histogram. To test the hypothesis that the observed and calculated distributions are really the same, χ^2 must be calculated by,

$$\chi^2 = \sum_{i=1}^{m} \frac{(f_i - e_i)^2}{e_i}, \quad (15) \qquad (21)$$

where f_i = the observed frequency and e_i = the expected frequency. The hypothesis can be accepted if $\chi^2 < \chi^2_{\alpha, m-2}$, where $\chi^2_{\alpha, m-2}$ is chi-square with a confidence level $1-\alpha$ and $m-2$ degrees of freedom. In this case, $m = 7$ and for a 95% confidence level, $\chi^2_{.05,5} = 9.488$. χ^2 was calculated for several assumed values of β. The best fit was found for $\beta = 0.28$, where $\chi^2 = 5.57 < 9.488$. Therefore, the hypothesis that the measured and calculated distributions are the same can be accepted.

2. Determination of K_1 and β from hard axis magnetization curves

The general method for finding K_1 and β is to compare the family of calculated curves generated by solving the integrals given in section D to the experimental hard axis magnetization curves. Values of K_1 and β are chosen to give the best agreement between experimental and calculated curves.

A computer program has been developed that compares an experimental curve to the calculated curve generated for each for a selected range of K_1. The program calculates a quantity

which measures the goodness of fit for each combination of K_1 and β. The program is listed in program 3. The main functions of the program are as follows:

1. Fit the calculated curves into parabolas of the form $m=A+Bh+Ch^2$. Parabolas are used here simply as a means of interpolation to obtain values of m for specific values of h. Plotting the calculated curves shows that they are nearly linear for the low values of h encountered in this calculation, i.e., $h<.5$, so that parabolic interpolation gives good accuracy without excessively complicating the process of calculating goodness of fit.

2. Convert all experimental data points to reduced coordinates for the selected range of K_1.

3. Square and sum the difference between the theoretically calculated and the measured magnetizations for each point taken from the experimental curve and print the sum for each pair of (K_1,β). In deciding the best values of K_1 and β, greatest weight is given to data taken at higher fields, since in this region the magnetization should change by rotation rather than by wall motion and the calculated curves assume only rotation. In practice, the decreasing field magnetization is measured at 100, 90, 80, 60, 40, and 20 kOe. In some cases, the magnetization measured at 20 kOe is dropped from the data to give better fit. This implies that domain wall motion becomes significant at approximately 20 kOe.

By examining the print-out to find a minimum in the goodness of fit criterion, the combination of K_1 and β can be found that yields the best agreement between experimental and calculated curves. Figure 12 shows a comparison of an experimental curve and the fitted calculated curve.

PROGRAM 3

```
10 DIM H(10),A(10),B(10),C(30),D(30),E(30)
15 PRINT "GOOD FIT PROGRAM, MODIFICATION 1-5-76"
18 FOR I=1 TO 27
20 READ C(I),D(I),E(I)
22 NEXT I
24 PRINT
25 READ Q
26 FOR L=1 TO Q
30 READ M,N,K1,K2
35 PRINT "#";L;"      (* 1E-04)      B=.18 TO .26"
40 FOR J=1 TO N
45 READ B(J),A(J)
47 A(J)=A(J)/M
50 NEXT J
55 Z=1
60 FOR K=K1 TO K2 STEP 1.000000E+07
65 PRINT INT(K/1.000000E+07+.5);
70 FOR I=Z TO 8+Z
75 S=0
80 FOR J=1 TO N
85 H(J)=B(J)*500*M/K
90 D=C(I)+D(I)*H(J)+E(I)*H(J)*H(J)-A(J)
95 S=S+D*D/N
100 IF S>5.000000E-04GO TO 160
110 NEXT J
150 PRINT TAB(7*(I-Z)+4);INT(S*1.000000E+07+.5)/10000;
160 NEXT I
165 PRINT
170 NEXT K
175 IF Z=19GO TO 225
180 PRINT
185 Z=Z+9
190 IF Z=10 THEN PRINT "B=.27 TO .35"
195 IF Z=19 THEN PRINT "B=.36 TO .44"
200 GO TO 60
225 PRINT \PRINT
250 NEXT L
300 DATA .1001,.9825,-.1372,.1055,.9817,-.1471,.111,.979,-.1507
 305 DATA .1164,.9771,-.1571,.1217,.975,-.1636,.1272,.972,-.1671
 310 DATA .13255,.9695,-.1707,.1378,.9689,-.1807,.1431,.9666,-.1871
 315 DATA .1484,.963,-.19,.1537,.961,-.1971,.1589,.9571,-.1971
 320 DATA .1639,.9565,-.2071,.1692,.9516,-.2071,.1744,.9485,-.2107
 325 DATA .1795,.946,-.2164,.1844,.9436,-.22,.1895,.9404,-.2243
 330 DATA .1944,.9371,-.2264,.1994,.9341,-.2307,.2042,.932,-.2371
 335 DATA .2091,.928,-.2372,.21411,.923,-.2364,.2188,.9215,-.2436
 340 DATA .2235,.9185,-.2471,.2283,.9139,-.2464,.233,.9104,-.2493
 999 END
```

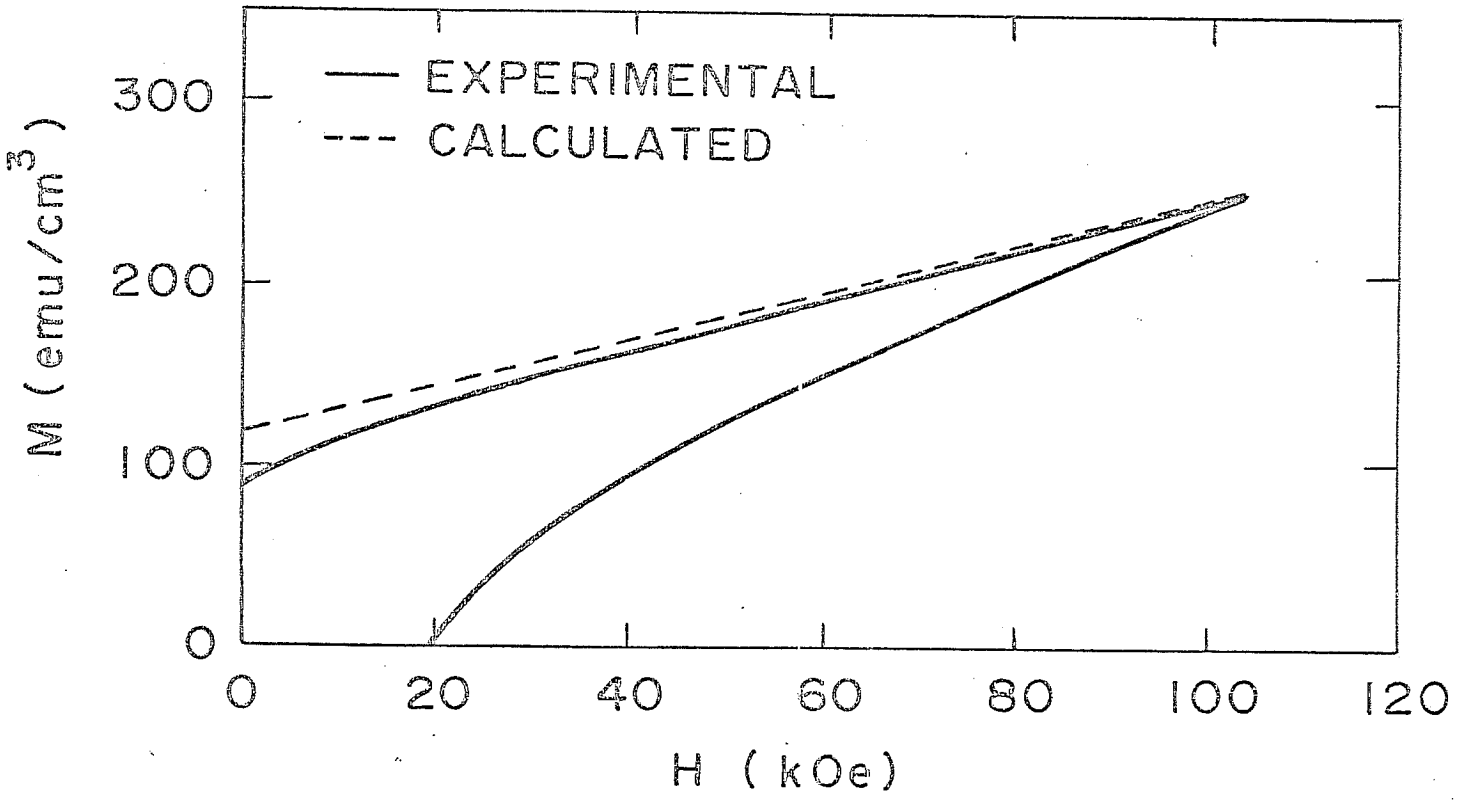

Figure 12. A comparison of experimental and calculated hard axis magnetization curves.

The calculated curve had to be drawn slightly above its true position to make the two curves appear distinct.

IV. RESULTS AND CONCLUSIONS

Numerical data are given in Table 4 and plotted in figures 13 through 16. The following points are worthy of note.

Figure 13 shows the coercive field to increase rapidly with decreasing temperature, approximately doubling between 300 and 77 K. Also, the coercivity is observed to increase between 77 and 4.2 K, contrary to the report of Benz and Martin.[3] The absolute value of H_{ci} in figure 14 is strongly dependent on composition, varying by almost two orders of magnitude from the best to the worst sample. The easy axis magnetic properties H_{ci}, M_s, M_r, and (BH)max are observed to peak near 16.8 atomic percent samarium (after correction is made for the formation of Sm_2O_3), corresponding to the samarium-rich side of the $SmCo_5$-Sm_2Co_7 phase boundary. This observation agrees with the conclusion of Martin, Benz, and Rockwood.[1] Also, the composition for maximum coercivity is temperature independent. The values obtained for σ_s ($\sigma_s = M_s/\text{density}$) are slightly larger than the published single crystal value, σ_{so}=96.0 emu/gram, of Tatsumoto et al.[16]

The measured room temperature anisotropy, in figure 15, is independent of composition. The numerical value of 1.4×10^8 ergs/cm^3 is within the range of reported single crystal values of 1.05×10^8 ergs/cm^3 (16) and 1.8×10^8 ergs/cm^3 measured by Sankar et al[17] and in good agreement with the value of 1.19×10^8

TABLE 4

Sample	at % Sm	Density (g/cm^3)	σ_s (emu/g)	M_s (emu/cm^3)	M_r (emu/cm^3)	H_{ci} (kOe)	H_k (kOe)	(BH)max (MGOe)	K_1 ($x10^8$ ergs/cm^3)	β (radians)
A	16.24	7.14	97.6	682	663	0.34	0.2	3.77	1.2	0.40
				728	680	0.52	0.4	4.88	2.3	
				728	690	0.84	0.7	5.23	1.9	
D	16.60	7.47	98.9	738	723	1.08	1.0	8.24	1.3	0.29
				778	770	2.24	2.2	15.6	2.2	
				778	772	2.44	2.3	16.6	1.8	
E	16.72	7.66	100.	782	763	14.8	5.4	21.0	1.6	0.23
				827	776	25.2	10.4	23.1	3.3	
				827	744	26.6	10.9	21.5	2.0	
F	16.84	7.82	96.4	750	739	16.4	4.7	22.7	1.3	0.21
				778	765	30.0	9.8	24.5	2.6	
				778	765	32.4	10.7	23.8	2.7	
G	16.96	7.73	96.6	747	728	14.4	4.5	19.7	1.5	0.28
				787	712	27.0	8.8	18.6	2.6	
				787	716	28.6	9.3	19.2	3.0	
H	17.08	7.81	95.6	747	722	6.6	4.1	19.9	1.4	0.29
				750	732	14.1	8.0	22.0	2.0	
				750	691	14.7	8.6	21.8	2.1	
Hitachi SmCo		8.11	86.1	698	646	28.2	6.7	17.0	1.2	0.43
				710	667	43.5	28.8	19.1	1.5	
				710	676	42.8	13.9	20.2	1.6	
Hitachi SmCoGd		8.27	58.0	480	447	42.2	12.5	7.97	0.6	0.44
				473	442	65.0	43.9	5.68	0.9	
				473	435	67.0	41.2	6.63	1.4	

The three sets of values for each sample are at 300, 77 and 4.2 K.

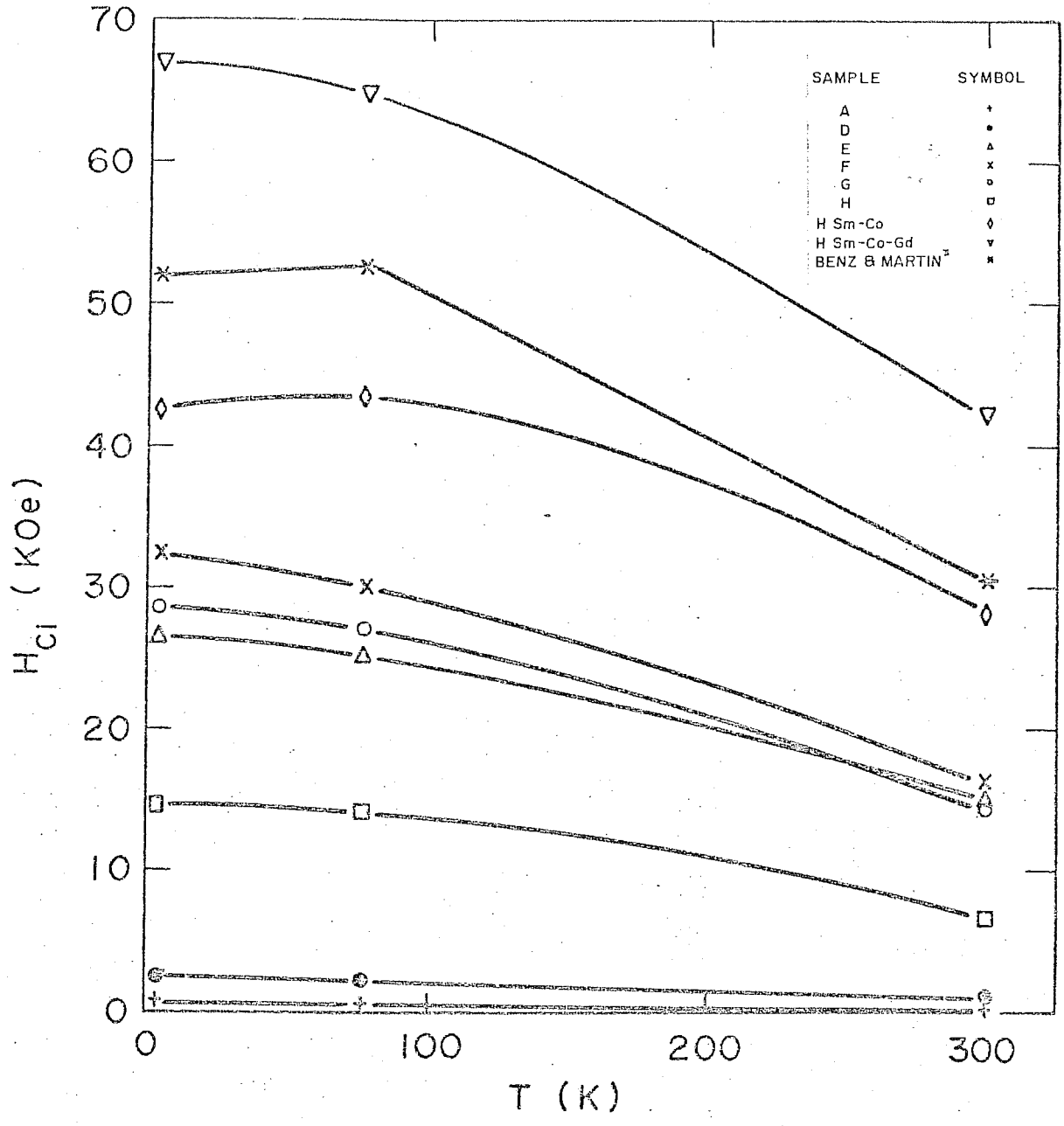

Figure 13. Intrinsic coercive field vs temperature.

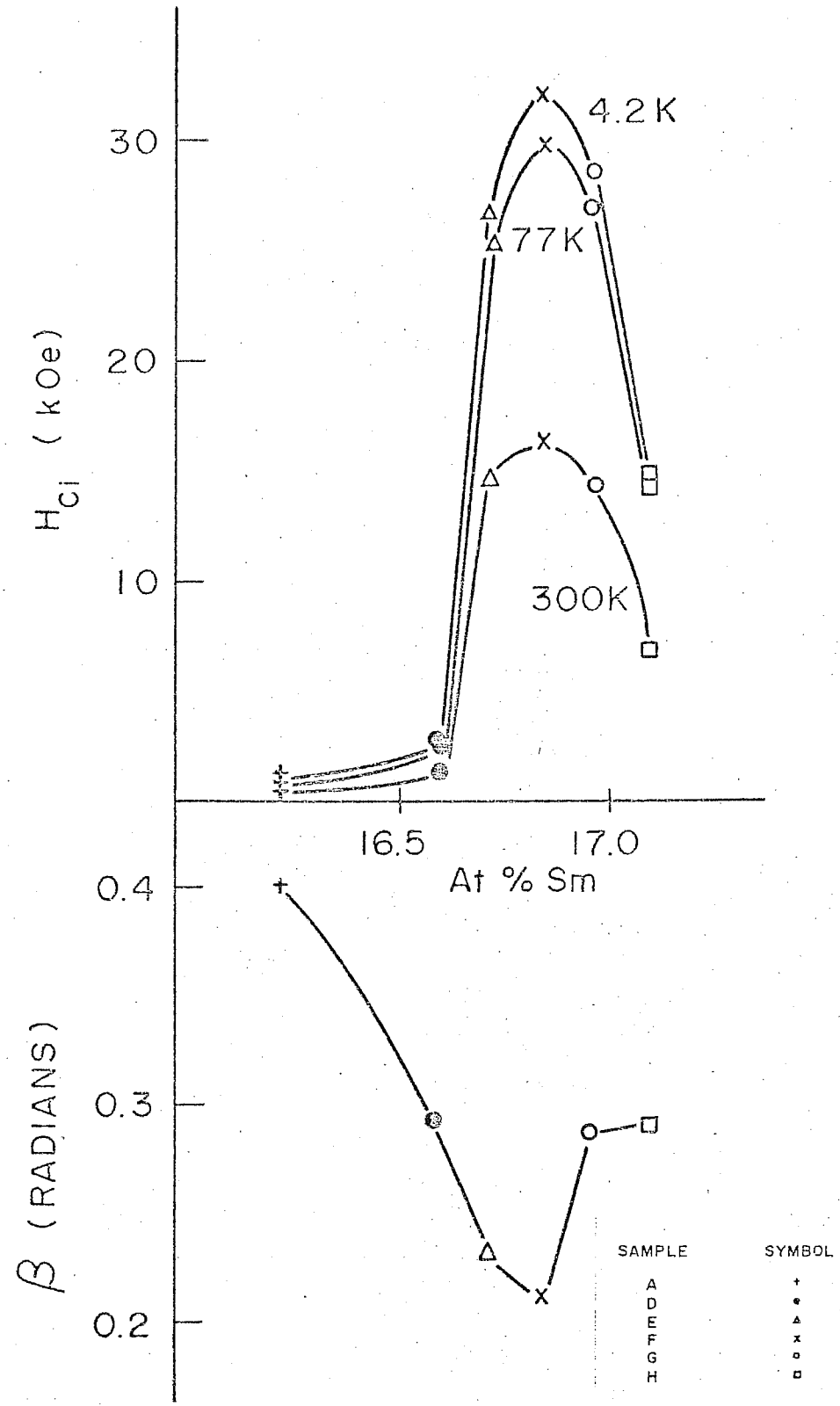

Figure 14. Intrinsic coercivity and particle misalignment vs composition.

ergs/cm^3 measured by Benz and Martin[3] for a sintered sample.

Figure 15 shows the measured K_1 to increase with decreasing temperature, approximately doubling between 300 and 77 K. Between 77 and 4.2 K, samples with low samarium content, A, D, and E, show an increase in anisotropy, while samples with high samarium content, F, G, and H, show a decrease in K_1. Sankar et al[17] reported a peak in anisotropy of their single crystal sample at 50 K; Benz and Martin[3] noted a drop in anisotropy from 77 to 4.2 K for their sintered sample. It is possible that the temperature at which the reported peak in anisotropy occurs is composition dependent, with the temperature for peak anisotropy increasing with increasing samarium content. It is also possible that the reported maximum in K_1 is an experimental problem due to insufficient applied field. The temperature dependence of the anisotropy reported here follows more closely the single crystal anisotropy temperature dependence[17] than did the Benz and Martin[3] study on a sintered sample. This could be due to the improved technique for measuring the anisotropy, as described in Section D of Chapter III.

The degree of particle misalignment, β, as shown in figures 14 and 16, is minimum in the General Electric samples of highest H_{ci} and M_s. The general quality of $SmCo_5$ as a permanent magnet correlates with the perfection of particle alignment, for the General Electric samples. It is interesting to note that the Hitachi samples show relatively poor alignment compared to the General Electric samples, yet the Hitachi samples have large coercivities.

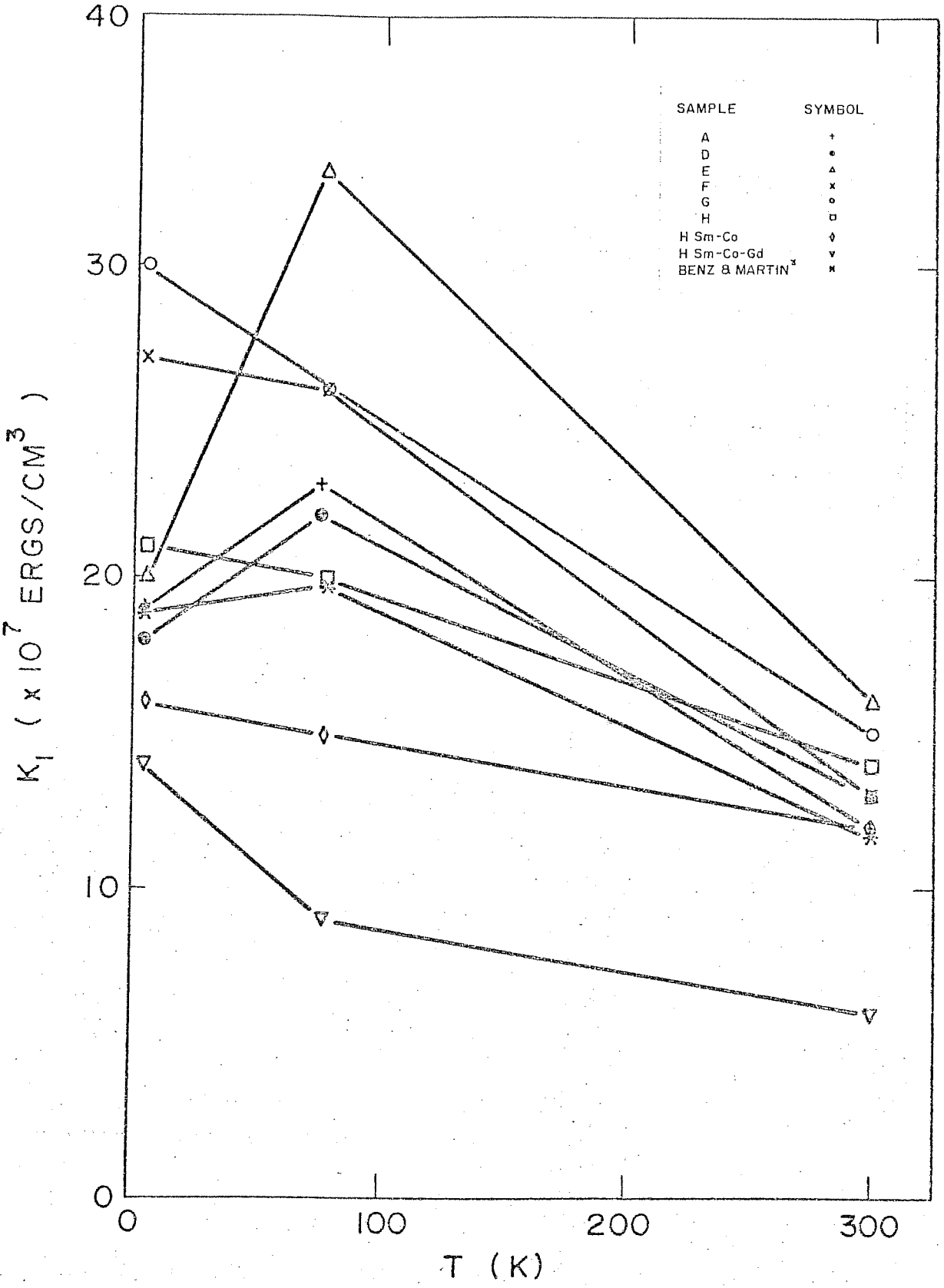

Figure 15. Anisotropy vs temperature.

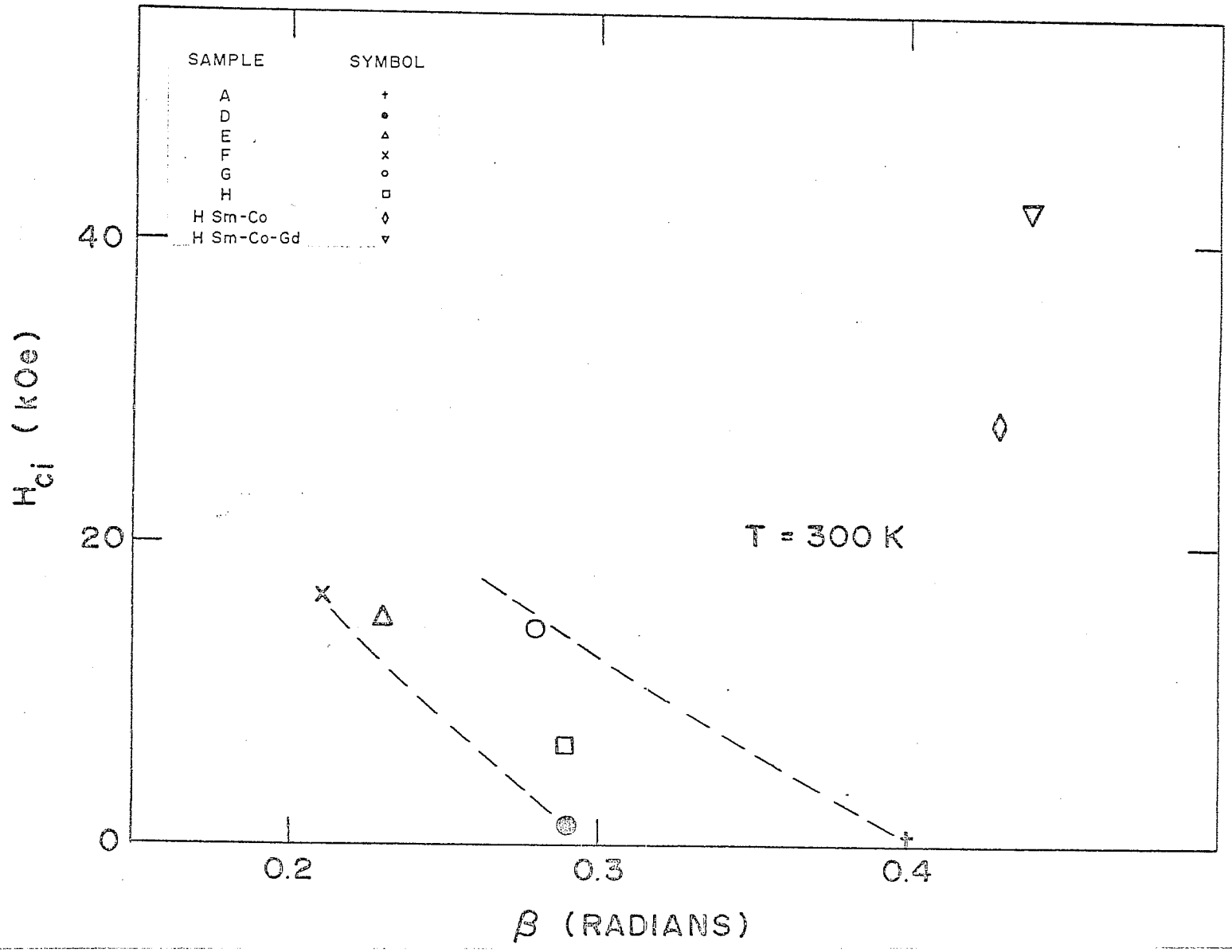

Figure 16. Intrinsic coercivity vs particle misalignment.

The results, as plotted in figure 17, show clearly that H_{ci} does not depend directly on the bulk anisotropy, contrary to the suggestion of Benz and Martin.[3] While it appears generally true that the higher the anisotropy, the higher the coercive field for a given sample, there is no consistently sloped linear relationship between K_1 and H_{ci}. It is interesting that the only sample whose points lie above the results of Benz and Martin is the Hitachi sample containing gadolinium. It is also interesting that the only sample to match the Benz and Martin data is the Hitachi sample with $SmCo_5$. It should also be noted that the low coercivity point on the Benz and Martin data in figure 17 was found at 500 K. If H_{ci} is controlled by a domain wall nucleation or pinning event, it is reasonable that H_{ci} would have the temperature dependence of the domain wall energy, which will be approximately the same as the temperature dependence of $K_1^{\frac{1}{2}}$. But the magnitude of H_{ci} will depend on some highly local structure and need not correlate with the magnitude of K_1.

Besides measuring the permanent magnet properties of sintered $SmCo_5$, this work has developed a new method for measuring the anisotropy constant K_1, and the degree of misorientation for sintered magnets. A family of calculated curves has been generated predicting the decreasing field portion of hard axis magnetization curves. The agreement with experimental curves is excellent at fields of 20 kOe or larger where there is no domain wall motion. Also, the assumed distribution of particle easy axes with respect to the alignment direction equation (4),

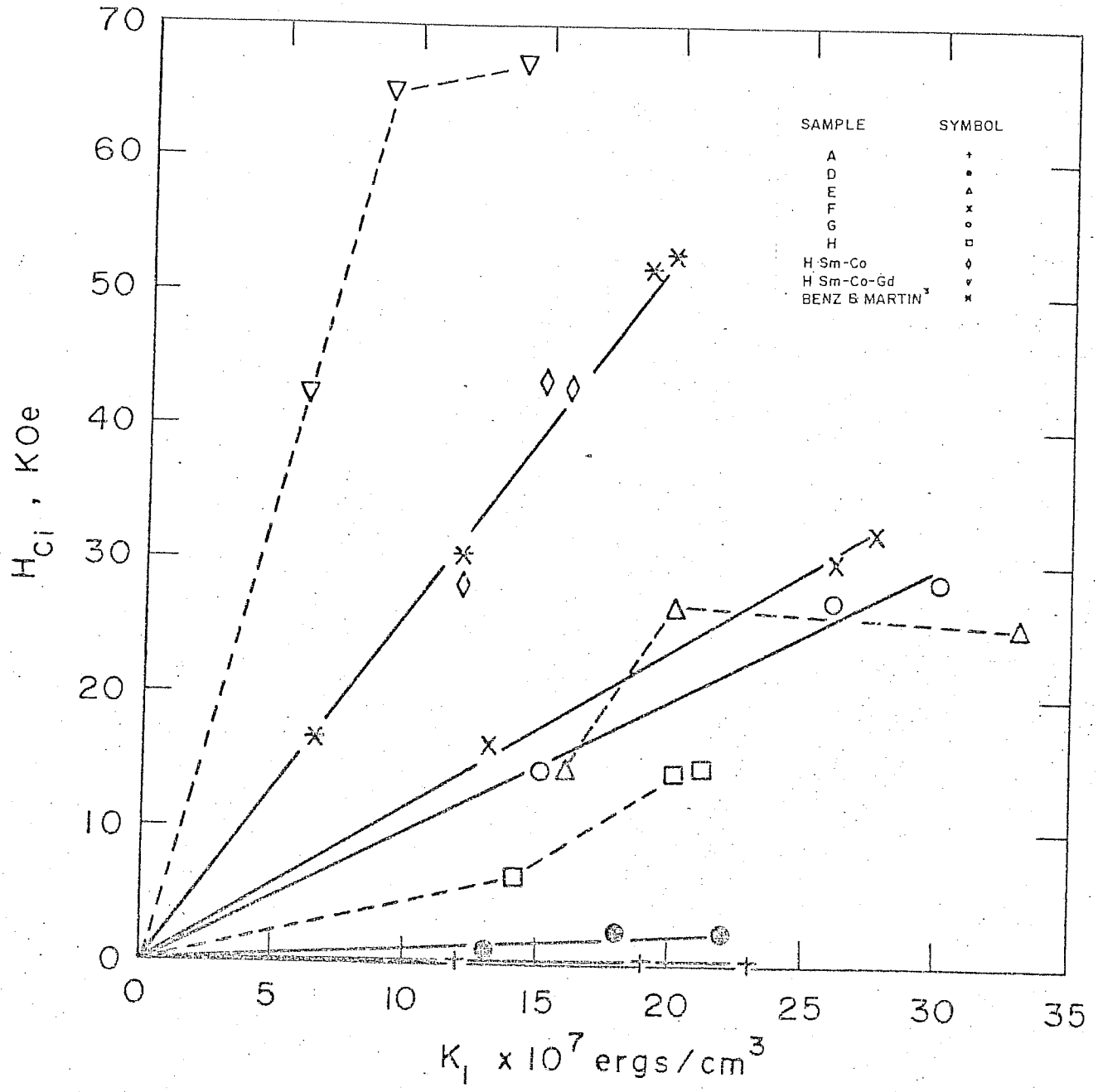

Figure 17. Intrinsic coercive field vs anisotropy.

has shown agreement with an independent experiment to measure the texture of sintered $SmCo_5$.

V. ACKNOWLEDGMENTS

This work was supported by the National Science Foundation through the Laboratory for Research on the Structure of Matter under contract DMR 72-03025. I am grateful to Professor C. D. Graham, Jr. for his constant help and guidance during this research. I would also like to express my thanks to Dr. D. L. Martin for providing the samples and for his helpful discussions, to Dr. T. Egami, P. J. Flanders, and L. Cheskis for their assistance with the experiments and to T. Schofield and B. Hui for their help with the statistical analysis. Finally, I want to thank my wife for her encouragement and cooperation, especially for typing this manuscript.

VI. REFERENCES

1. D. L. Martin, M. G. Benz, and A. C. Rockwood, AIP Conf. Proc. 10 (1973) 583.

2. D. L. Martin, to be published in 1976 AIP Conf. Proceedings.

3. M. G. Benz and D. L. Martin, J. Appl. Phys. 43 (1972) 4733.

4. G. W. Urbain, P. Weiss, and F. Trombe, Comptes Rendus 200 (1935) 2132.

5. K. Nassau, L. V. Cherry, and W. E. Wallace, J. Phys. Chem. Solids 16 (1960) 123.

6. W. M. Hubbard, E. Adams, and J. V. Gilfrich, J. Appl. Phys. 31 (1960) 3683.

7. G. Hoffer and K. Strnat, IEEE Trans. Magnetics 2 (1966) 487.

8. D. L. Martin and M. G. Benz, AIP Conf. Proc. 5 (1972) 970.

9. E. A. Nesbitt and J. H. Wernick, Rare Earth Permanent Magnets, Academic Press, New York (1973) p. 80.

10. J. D. Livingston, AIP Conf. Proc. 10 (1973) 643.

11. D. L. Martin, private communication.

12. M. G. Benz and D. L. Martin, Appl. Phys. Lett. 17 (1970) 176.

13. B. D. Cullity, Introduction to Magnetic Materials, Addison-Wesley, Reading, Mass. (1972) p. 228.

14. A. M. Legendre, Exercises De Calcul Integral, vol. I, Paris, Coureier (1811) p. 363.

15. J. E. Freund, Mathematical Statistics, Prentice-Hall, Englewood Cliffs, N. J. (1971) pp. 171, 172, and 338.

16. E. Tatsumoto, J. Okamoto, H. Fuji, and C. Inoue, Suppl. J. Physique 32 (1971) C1-550.

17. S. G. Sankar, V. U. S. Rao, E. Segal, W. E. Wallace, W. G. Frederick, and H. J. Garrett, Phys. Rev. 11 (1975) 435.

VII. APPENDIX

This paper was presented at the 1975 Conference on Magnetism and Magnetic Materials and will be published in the 1976 AIP Conference Proceedings.

HIGH FIELD MAGNETIC MEASUREMENTS ON SINTERED $SmCo_5$ PERMANENT MAGNETS

Stanley R. Trout and C. D. Graham, Jr.
Department of Metallurgy and Materials Science and
Laboratory for Research on the Structure of Matter
University of Pennsylvania, Philadelphia, Pa 19174

ABSTRACT

Hysteresis loops in fields to 100 kOe have been measured at 300, 77, and 4.2K parallel and perpendicular to the alignment axis in a series of sintered $SmCo_5$ magnets with compositions varying from 16.24 to 17.08 at% Sm. Analysis of the data taken perpendicular to the alignment axis permits evaluation of the effective anisotropy constant K_1, and also the degree of misorientation of the individual particles. Intrinsic coercive fields H_{ci} varied from 0.34 to 16.4 kOe at room temperature. In all samples, H_{ci} and K_1 increased rapidly with decreasing temperature, roughly doubling between room temperature and 77K. This confirms more generally the result reported for two samples by Benz and Martin.[1] The values of H_{ci} and $(BH)_{max}$ depend strongly on composition, but the anisotropy does not. Variations in permanent magnet properties are therefore not directly related to variations in the bulk anisotropy.

INTRODUCTION

Benz and Martin[1] measured the magnetic properties of several sintered $SmCo_5$ magnets as a function of temperature and made the surprising observation that H_{ci} increased linearly with decreasing temperature, following quite closely the linear increase in K_1. The coercive field in these magnets is usually attributed to domain wall nucleation or pinning effects that are structure sensitive[2] and not necessarily linearly dependent on the bulk crystal anisotropy.

The present investigation was undertaken to see whether this temperature dependence of H_{ci} is general for $SmCo_5$ magnets, and more broadly to add to the understanding of the coercive field and the permanent magnet properties of $SmCo_5$ and related materials. The experiments also gave information about the degree of alignment of the individual particles in sintered magnets.

SAMPLES AND EXPERIMENTAL PROCEDURE

A series of samples covering the composition range from 16.24 to 17.08 at% Sm ($SmCo_{5.16}$ to $SmCo_{4.85}$) was obtained from D. L. Martin of the GE Research and Development Center. These are the same samples whose room-temperature properties were reported by Martin, Benz, and Rockwood[3]; they show a wide range of quality as permanent magnets. Magnetization curves and hysteresis loops were measured parallel and perpendicular to the alignment axis at 300, 77, and 4.2K on cube samples of 3.2 mm size in fields to 100 kOe using a mechanically-driven vibrating sample magnetometer. The demagnetizing factor was taken as $4\pi/3$, a value confirmed by measurements on an iron cube in the same apparatus. Magnetic saturation could not be attained in all samples at low temperatures even at 100 kOe, so the low temperature saturations were obtained from the room temperature values and the single-crystal temperature dependence.[4]

Conventional permanent magnet properties were obtained from the easy axis magnetization data, and the effective bulk anisotropy was determined from the hard-axis data. A perfectly-oriented single crystal with anisotropy described by a single constant ($E_K=K_1 \sin^2\theta$) has a linear hard-axis magnetization curve with slope $M_s^2/2K_1$. In sintered magnets, the alignment of the individual particles is not perfect, so more complex magnetization curves result. The linear hard-axis curve reported by Benz and Martin[1] were obtained by first magnetizing the samples in the easy direction to minimize domain wall motion. We chose instead to fit the hard axis curves measured in decreasing fields to a calculated curve in which there are two adjustable parameters: the uniaxial anisotropy constant K_1 and an angle β which measures the distribution of the polar angles ϕ (see Fig. 1) between the particle axes and the alignment axis. The angle ϕ is assumed to be described by a spherical normal distribution, $f(\phi)=k\exp(-\phi^2/\beta^2)$, where k is a normalization constant. Direct observation by Martin[5] show this assumption to be reasonable. The distribution of particle axes is assumed independent of the azimuthal angle θ. To a first approximation, the standard deviation of ϕ is related to β by $\sigma = \beta(1-\frac{\pi}{4})$.

A field applied perpendicular to the alignment axis causes the magnetization of the particle to rotate by an angle γ towards H. The angle γ is determined by a balance between the torque from the field $L=M_s H \sin(\lambda-\gamma)$ and the torque from the anisotropy $L=-dE_K/d\phi=-K_1 \sin 2\gamma$. The resulting magnetization is given by

$$M=M_s\int_0^{2\pi}\int_0^{\pi/2} f(\phi)\cos(\lambda-\gamma)\sin\phi\, d\phi\, d\theta=f(H,K_1,\beta). \quad (1)$$

Tables of M/M_s were calculated for a series of values of $h=HM_s/2K_1$ and β, and the experimental hard-axis curves were fitted to the calculated values to obtain the quantities K_1 and β. In the fitting, greatest weight was given to the high field data, since in this region the magnetization should change by rotation rather than by wall motion, and the calculated curves assume only rotation.

RESULTS AND CONCLUSIONS

Numerical data are given in Table I and plotted in Figs. 2 and 3. The following points are worthy of note.

The coercive field increases rapidly with decreasing temperature in all samples, approximately doubling between 300 and 77K. The absolute value of H_{ci}, however, is strongly dependent on composition, varying by almost a factor of 50 from the best to the worst sample. Maximum H_{ci} is observed at about 16.8 at% Sm, in agreement with Martin, Benz, and Rockwood,[3] and the composition for maximum H_{ci} does not change with temperature of measurement.

The room-temperature anisotropy is almost independent of composition, and the numerical value of about 1.5×10^8 erg/cm^3 is in reasonable agreement with single-crystal values.[4,6] The measured K_1 increases with decreasing temperature, approximately doubling between 300 and 77K. There is serious scatter in the values of K_1 at 4.2K. This may be experimental error caused by the increasing difficulty of saturating the magnetization as the anisotropy increases; however, other investigators have found the anisotropy to drop at low temperatures.[1,4,6]

The degree of particle misalignment β is minimum in the samples of highest H_{ci}, but it is hard to say if there is any causal relation between the two quantities.

The results show clearly that H_{ci} does not depend directly on the bulk anisotropy, contrary to the suggestion of Benz and Martin.[1] If H_{ci} is controlled by a domain wall nucleation or pinning event, it is reasonable that H_{ci} would have the temperature dependence of the domain wall energy, which will be approximately the same as the temperature dependence of $K_1^{\frac{1}{2}}$. But the magnitude of H_{ci} will depend on some highly local structure and need not correlate with the magnitude of K_1.

ACKNOWLEDGEMENTS

This work was supported by the National Science Foundation through the Laboratory for Research on the Structure of Matter under contract DMR 72-03025. We are grateful to D. L. Martin for providing the samples and to P. J. Flanders for assistance with the experiments.

REFERENCES

1. M. G. Benz and D. L. Martin, J. Appl. Phys. 43 4733 (1972).
2. J. D. Livingston, AIP Conf. Proc. 10 643 (1973).
3. D. L. Martin, M. G. Benz, and A. C. Rockwood, AIP Conf. Proc. 10 583 (1973).
4. E. Tatsumoto, J. Okamoto, H. Fuji, and C. Inoue, Suppl. J. de Physique 32 C1-550 (1971).
5. D. L. Martin, private communication.
6. S. G. Sankar, V. U. S. Rao, E. Segal, W. E. Wallace, W. G. Frederick, and H. J. Garrett, Phys. Rev. 11 435 (1975).

TABLE I

at% Sm	H_{ci} kOe	$(BH)_{max}$ MGOe	K_1 10^8 erg/cm^3	β rad
16.24	0.34	3.77	1.5	0.42
	0.52	4.88	2.8	0.39
	0.84	5.23	2.3	0.40
16.60	1.08	8.24	1.4	0.31
	2.24	15.6	2.6	0.29
	2.44	16.6	2.0	0.32
16.72	14.8	21.0	1.6	0.24
	25.2	23.1	3.5	0.22
	26.6	21.5	3.9	0.21
16.84	16.4	22.7	1.5	0.21
	30.0	24.5	3.7	0.22
	32.4	23.8	3.4	0.19
16.96	14.4	19.7	1.8	0.27
	27.0	18.6	2.8	0.24
	28.6	19.2	3.7	0.25
17.08	6.6	19.9	1.5	0.27
	14.1	22.0	3.1	0.28
	14.7	21.8	2.6	0.25

The three sets of values for each sample are at 300, 77, and 4.2K.

Fig. 1. Angles used in calculation of hard-axis magnetization curves. P is the axis of an individual particle. Angles ϕ and λ are not coplanar; angles γ and λ are coplanar.

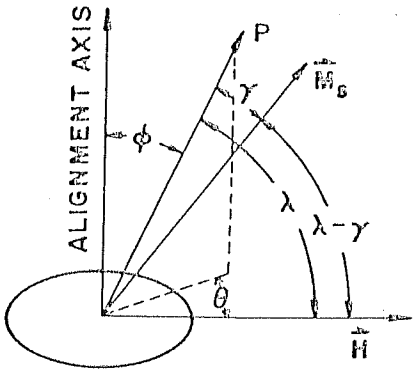

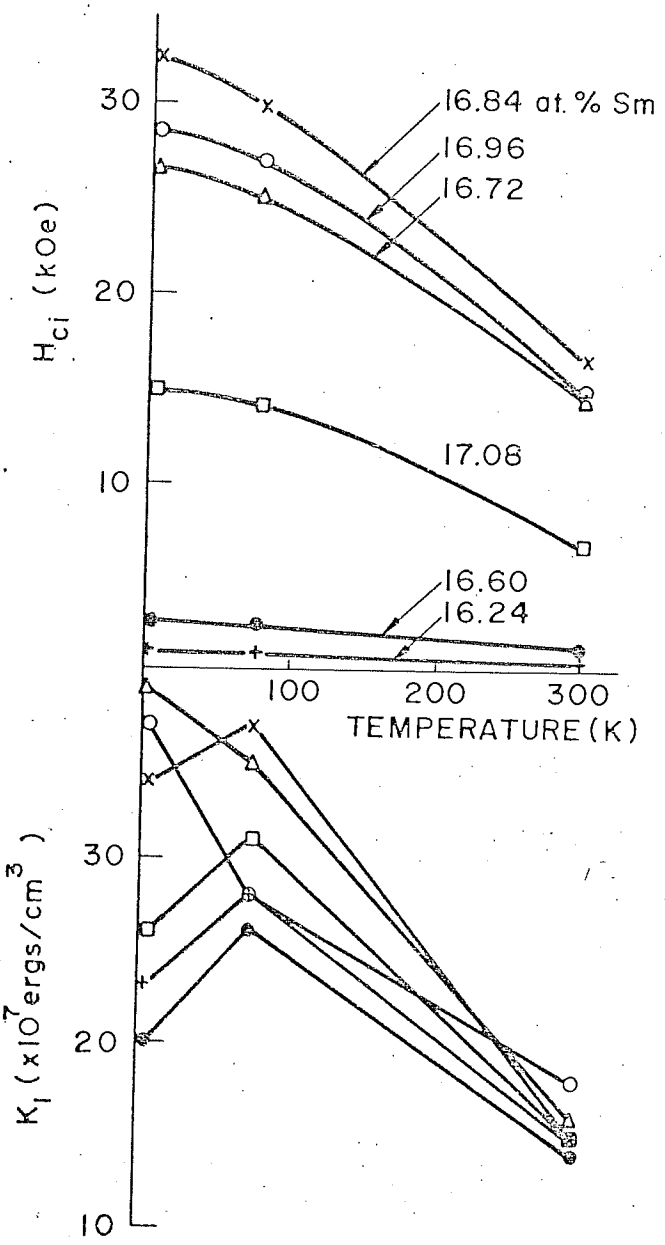

Fig. 2. H_{ci} and K_1 vs temperature for all samples.

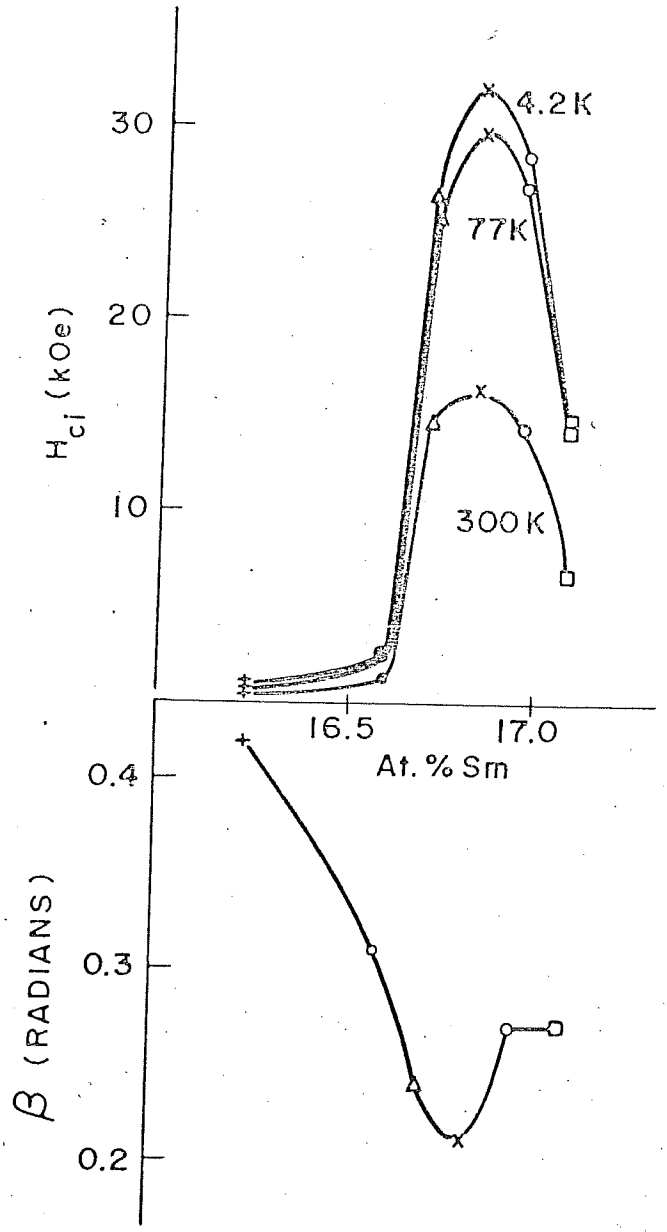

Fig. 3. H_{ci} (three temperatures) and average β vs composition.